



HAL
open science

Archaeal extracellular vesicles are produced in an ESCRT-dependent manner and promote gene transfer and nutrient cycling in extreme environments

Junfeng Liu, Virginija Cvirkaite-Krupovic, Pierre-Henri Commere, Yunfeng Yang, Fan Zhou, Patrick Forterre, Yulong Shen, Mart Krupovic

► To cite this version:

Junfeng Liu, Virginija Cvirkaite-Krupovic, Pierre-Henri Commere, Yunfeng Yang, Fan Zhou, et al.. Archaeal extracellular vesicles are produced in an ESCRT-dependent manner and promote gene transfer and nutrient cycling in extreme environments. *The International Society of Microbiological Ecology Journal*, 2021, 15 (10), pp.2892-2905. 10.1038/s41396-021-00984-0 . pasteur-03209564

HAL Id: pasteur-03209564

<https://pasteur.hal.science/pasteur-03209564>

Submitted on 27 Apr 2021

HAL is a multi-disciplinary open access archive for the deposit and dissemination of scientific research documents, whether they are published or not. The documents may come from teaching and research institutions in France or abroad, or from public or private research centers.

L'archive ouverte pluridisciplinaire **HAL**, est destinée au dépôt et à la diffusion de documents scientifiques de niveau recherche, publiés ou non, émanant des établissements d'enseignement et de recherche français ou étrangers, des laboratoires publics ou privés.



Distributed under a Creative Commons Attribution - NonCommercial 4.0 International License

1 **Archaeal extracellular vesicles are produced in an ESCRT-dependent manner and promote gene**
2 **transfer and nutrient cycling in extreme environments**

3
4
5
6 Junfeng Liu^{1,2}, Virginija Cvirkaite-Krupovic², Pierre-Henri Commere³, Yunfeng Yang¹, Fan Zhou¹, Patrick
7 Forterre², Yulong Shen¹, Mart Krupovic^{2*}

8
9 ¹ CRISPR and Archaea Biology Research Center, State Key Laboratory of Microbial Technology,
10 Microbial Technology Institute, Shandong University, Qingdao, China

11 ² Archaeal Virology Unit, Institut Pasteur, 75015 Paris, France

12 ³ Institut Pasteur, Flow Cytometry Platform, 75015 Paris, France

13
14
15
16 * – Correspondence to:

17 Mart Krupovic

18 Archaeal Virology Unit,

19 Department of Microbiology, Institut Pasteur,

20 75015 Paris, France

21 E-mail: mart.krupovic@pasteur.fr

22 Tel: 33 (0)1 40 61 37 22

23
24
25
26 **Running title:**

27 Role of extracellular vesicles in extreme environments

28
29 **Competing Interests**

30 The authors declare that they have no competing interests.

31

32 **ABSTRACT**

33 Membrane-bound extracellular vesicles (EVs), secreted by cells from all three domains of life,
34 transport various molecules and act as agents of intercellular communication in diverse
35 environments. Here we demonstrate that EVs produced by a hyperthermophilic and acidophilic
36 archaeon *Sulfolobus islandicus* carry not only a diverse proteome, enriched in membrane proteins,
37 but also chromosomal and plasmid DNA, and can transfer this DNA to recipient cells.
38 Furthermore, we show that EVs can support the heterotrophic growth of *Sulfolobus* in minimal
39 medium, implicating EVs in carbon and nitrogen fluxes in extreme environments. Finally, our
40 results indicate that, similar to eukaryotes, production of EVs in *S. islandicus* depends on the
41 archaeal ESCRT machinery. We find that all components of the ESCRT apparatus are
42 encapsidated into EVs. Using synchronized *S. islandicus* cultures, we show that EV production is
43 linked to cell division and appears to be triggered by increased expression of ESCRT proteins
44 during this cell cycle phase. Using a CRISPR-based knockdown system, we show that archaeal
45 ESCRT-III and AAA+ ATPase Vps4 are required for EV production, whereas archaea-specific
46 component CdvA appears to be dispensable. In particular, the active EV production appears to
47 coincide with the expression patterns of ESCRT-III-1 and ESCRT-III-2, rather than ESCRT-III,
48 suggesting a prime role of these proteins in EV budding. Collectively, our results suggest that
49 ESCRT-mediated EV biogenesis has deep evolutionary roots, likely predating the divergence of
50 eukaryotes and archaea, and that EVs play an important role in horizontal gene transfer and
51 nutrient cycling in extreme environments.

52

53 **Keywords:** Archaea, extracellular vesicles, ESCRT system, hyperthermophiles, *Saccharolobus*
54 *solfataricus*

55 INTRODUCTION

56 Extracellular vesicles (EVs) are membrane-bound particles of variable diameter secreted by the cells into
57 extracellular milieu. Although known for several decades, EVs were broadly regarded as cellular waste
58 products, debris or artifacts of lipid aggregation [1]. However, the growing body of data shows that EVs
59 play multiple, biologically important roles in all three domains of life [1-7]. During the past decade, it was
60 discovered that EVs are responsible for intercellular shuttling of diverse cargoes, including proteins, DNA,
61 RNA, lipids and various signaling molecules [5, 7-10], and may promote certain human pathologies [11,
62 12], including cancer [13, 14]. Furthermore, EVs hold great promise as vehicles for drug targeting and
63 delivery [15, 16]. Finally, EVs may play an important ecological role, especially, in aquatic ecosystems [5].
64 It has been shown that DNA-carrying EVs produced by diverse bacteria, including *Prochlorococcus*, a
65 numerically dominant marine cyanobacterium, are abundant in coastal and open-ocean seawater samples
66 [7]. Importantly, *Prochlorococcus* EVs could support the growth of heterotrophic bacterial cultures, which
67 implicates EVs in marine carbon flux [7]. Archaea of the phyla Euryarchaeota and Crenarchaeota are also
68 known to produce EVs under laboratory conditions. *Thermococcus prieurii*, but not other *Thermococcus*
69 species, secrete EVs packed with elemental sulfur, presumably to prevent the accumulation of toxic levels
70 of sulfur in the cytoplasm [17]. Furthermore, similar to bacteria, EVs produced by members of the phylum
71 Euryarchaeota thriving in deep-sea hydrothermal vents (order Thermococcales) and saline lakes (order
72 Halobacteriales) were shown to carry DNA [18-21]. Whether the same is true for EVs produced by
73 crenarchaea of the order Sulfolobales, which represent major inhabitants of terrestrial acidic hot springs,
74 remains unknown. It is also unclear whether archaeal EVs are secreted under natural growth conditions in
75 the environment.

76
77 The mechanisms of EV biogenesis have been extensively studied in eukaryotes but remain poorly
78 understood in bacteria and archaea [1, 3]. In eukaryotes, the most studied mechanism of EV formation relies
79 on the endosomal sorting complex required for transport (ESCRT) machinery [22-24]. Many archaea also
80 encode homologs of the ESCRT system but its involvement in EV biogenesis remains unclear. The ESCRT
81 machinery is responsible for many key membrane remodeling processes in eukaryotic cells, including
82 membrane abscission during cytokinesis, biogenesis of certain types of EVs and multivesicular bodies, and
83 budding of enveloped viruses, such as HIV-1 and Ebola virus [22, 25, 26]. The ESCRT proteins assemble
84 on the cytosolic face of the membrane and drive membrane bending and scission reaction [26]. The ESCRT
85 machinery can be subdivided into several functionally distinct subcomplexes known as ESCRT-0, ESCRT-
86 I, ESCRT-II and ESCRT-III as well as AAA+ ATPase Vps4. Among these, ESCRT-III and Vps4 are
87 universally involved in ESCRT-dependent membrane remodeling processes, whereas ESCRT-0, ESCRT-I
88 and ESCRT-II are compartment-specific and facilitate recruitment of ESCRT-III to diverse membranes in
89 different cellular contexts [25, 27]. ESCRT-III proteins form a ring-like filament at the membrane, whereas
90 the Vps4 ATPase binds directly to ESCRT-III and dynamically disassembles the ESCRT-III complex in an
91 ATP-dependent manner, thereby driving membrane-remodeling [28, 29].

92
93 Similar to eukaryotes, most archaea of the TACK (for Thaumarchaeota, Aigarchaeota, Crenarchaeota and
94 Korarchaeota) and Asgard superphyla encode an ESCRT machinery [30-33]. Interestingly, the ESCRT
95 machinery encoded by Asgard archaea is phylogenetically more closely related to the eukaryotic homologs
96 compared to those from other archaea and Asgard Vps4 could efficiently complement the *vps4* null mutant
97 of *Saccharomyces cerevisiae* [31, 34]. However, due to difficulties in cultivation and lack of genetic tools
98 in Asgard archaea, the role of their ESCRT machinery in membrane remodeling remains to be investigated
99 in this superphylum. The archaeal ESCRT system has been experimentally investigated in *Sulfolobus* and
100 *Nitrosopumilus* species [33, 35-41], with *Sulfolobus* representing the model organism for elucidation of the
101 role and functioning of the archaeal ESCRT machinery [30, 41, 42]. In hyperthermophilic archaea of the
102 order Sulfolobales, the ESCRT machinery is the key component of cell division apparatus composed of
103 AAA+ ATPase Vps4 (also known as CdvC), four ESCRT-III homologs (ESCRT-III [CdvB], ESCRT-III-
104 1 [CdvB1], ESCRT-III-2 [CdvB2], ESCRT-III-3 [CdvB3]), and archaea-specific component CdvA. The
105 latter protein binds to DNA [43, 44] and recruits ESCRT-III to the membrane [44]. CdvA is not homologous

106 to the eukaryotic ESCRT-0, ESCRT-I or ESCRT-II [45], and is missing in certain archaea, including some
107 thaumarchaea [46] and euryarchaea [47]. Recently, it has been demonstrated that ESCRT machinery also
108 mediates asymmetric cell division via budding in virus-infected *S. islandicus* cells [48]. It has been also
109 proposed that the *Sulfolobus* ESCRT machinery is involved in viral assembly within the cytoplasm and in
110 escape from the infected cell by using a unique lysis mechanism [49]. Whether the function of archaeal
111 ESCRT machinery can be extended to other membrane remodeling processes, such as budding of enveloped
112 viruses [50] and EVs [3], remains to be demonstrated. Notably, ESCRT-III-1, ESCRT-III-2 and Vps4 were
113 identified among proteins present within EVs secreted by *Sulfolobus acidocaldarius*, *S. solfataricus* and *S.*
114 *tokodaii* [51]. This finding suggested that ESCRT machinery is involved in EV biogenesis [51]. However,
115 EVs are known to be produced by archaea which lack the functional ESCRT system and divide using the
116 bacterial-like FtsZ-based cell division machinery, including halophilic archaea (class Halobacteria) and
117 members of the order Thermococcales [18, 52].

118
119 Here we characterize the composition, role and biogenesis of EVs produced by a hyperthermophilic and
120 acidophilic archaeon *Sulfolobus islandicus*. We demonstrate that besides proteins, *Sulfolobus* EVs carry
121 chromosomal and plasmid DNA, and that EVs can transfer this DNA to recipient cells. We also investigate
122 the role of the *Sulfolobus* ESCRT machinery in EV biogenesis and show that all four ESCRT-III homologs
123 and Vps4 ATPase play an important role in this process, whereas CdvA appears to be dispensable. Using
124 synchronized *S. islandicus* cultures, we demonstrate that EV production is linked to cell division and
125 appears to follow the cell cycle-coordinated fluctuations in the expression of ESCRT proteins. Finally, we
126 show that EVs similar to those produced by *Sulfolobus* cells under laboratory conditions can be also found
127 in the environmental sample. Collectively, our results suggest that the ESCRT-dependent mechanism of
128 EV biogenesis is conserved in the archaeo-eukaryotic lineage and that EVs play an important role in gene
129 transfer in extreme environments.

130

131 **RESULTS AND DISCUSSION**

132 **EV production and purification**

133 To study the composition and function of archaeal EVs, and to investigate the role of ESCRT in their
134 biogenesis, we established a procedure for purification and quantification of EVs from *Sulfolobus*
135 *islandicus* REY15A and *Saccharolobus solfataricus* PH1 cells (Sis-EVs and Sso-EVs, respectively), and
136 compared the EV production at different growth stages in both strains. Consistent with the observations
137 made for EVs isolated from other *Sulfolobus* species [51], Sis-EVs and Sso-EVs were visibly coated with
138 the proteinaceous surface (S-)layer (Fig. 1a) typical of *Sulfolobus* cells [53, 54] and displayed considerable
139 variation in shape and diameter. The median diameters of Sis-EVs and Sso-EVs were 176.54 nm and 185.85
140 nm, respectively, with the Sso-EVs being slightly more variable in size (Fig. 1b). The EVs were collected
141 at different stages of cell growth (Fig. 1c) and could be reproducibly quantified by flow cytometry using
142 tubes containing a calibrated number of fluorescent beads (Fig. 1d and Fig. S1). With a notable exception
143 of the 12-hour time point, EV production by *S. islandicus* and *S. solfataricus* followed a similar pattern:
144 EV titer increased throughout the growth of the cells (Fig. 1c). Given the similarities in EV production
145 patterns in *S. islandicus* and *S. solfataricus*, for all subsequent experiments, we focused on EVs from *S.*
146 *islandicus*, for which more advanced genetic tools are available [55]. We next tested whether there is a link
147 between Sis-EV production and increase in the fraction of the dead cells in the growing *S. islandicus*
148 population by performing the live/dead staining at different time points (see Materials and Methods). From
149 12 to 60 h (early exponential to stationary phase) the ratio of dead cells remained at around 1% and only
150 when the cells progressed into the ‘death’ phase, the ratio of dead cells increased sharply, with around 30%
151 of dead cells at 72 h and more than 90% of dead cells at 84 h (Fig. S2). These results suggest that Sis-EVs
152 production is not a consequence of cell death. To verify that the EV preparations were devoid of cellular
153 contaminants, we performed the following procedures: (i) flow cytometry profiles of the EV samples were
154 compared with those containing *Sulfolobus* cells (Fig. S1); (ii) purified EV preparations were subjected to
155 semi-quantitative transmission electron microscopy analysis (Fig. S3a); (iii) EV preparations were also

156 analyzed by fluorescence microscopy (Fig. S3b); and (iv) EV preparations were plated on solid medium
157 supporting the growth of *Sulfolobus* cells (Fig. S4). None of these procedures revealed the presence of
158 *Sulfolobus* cells, viable or otherwise, in the EV preparations.

159

160 **Protein content of Sis-EVs**

161 EVs are known to carry diverse cargo, including proteins [2-5]. Proteomics analysis of Sis-EVs and *S.*
162 *islandicus* cells led to the identification of 413 and 1035 proteins, respectively (Supplementary Data 1).
163 The number of proteins detected in Sis-EVs is considerably higher than that reported previously for EVs
164 from *S. acidocaldarius*, *S. solfataricus* and *S. tokodaii* [51], possibly due to improved sensitivity of mass-
165 spectrometry over the past decade. Notably, recent studies on the proteomics of EVs produced by diverse
166 bacteria [56-59] as well as halophilic archaea [18] report the presence of hundreds of proteins in each type
167 of EVs, consistent with our results. For instance, it has been shown that EVs produced by halophilic
168 archaeon *Halorubrum lacusprofundi* contain 447 different proteins [18].

169

170 All but one functional protein categories found in *S. islandicus* proteome, as defined using the archaeal
171 clusters of orthologous groups (arCOG; Table S1) [60], were represented in the Sis-EVs (Fig. 2a). Proteins
172 of the arCOG category X (Mobilome: prophages, transposons) were not found in the Sis-EVs, likely due to
173 the fact that only few proteins of this functional category are expressed in *S. islandicus* under normal growth
174 conditions [61, 62]. The fractions of proteins of the categories J (Translation, ribosomal structure and
175 biogenesis), K (Transcription), V (Defense mechanisms), H (Coenzyme transport and metabolism) and I
176 (Lipid transport and metabolism) were more than twice smaller compared to their corresponding fractions
177 in the total cellular proteome. By contrast, arCOG categories D (Cell cycle control, cell division,
178 chromosome partitioning), N (Cell motility), O (Posttranslational modification, protein turnover,
179 chaperones), U (Intracellular trafficking, secretion, and vesicular transport), C (Energy production and
180 conversion), P (Inorganic ion transport and metabolism) and S (Function unknown) were enriched in Sis-
181 EVs compared to the total cellular proteome (Fig. 2a). For instance, the D category proteins constitute only
182 0.6% of the total *S. islandicus* proteome, whereas in Sis-EVs, these proteins correspond to 1.7% of proteins
183 (2.9-fold increase). There is also notable enrichment in Sis-EVs of proteins with predicted transmembrane
184 domains compared to the cellular proteome (20% vs 4%; Fig. 2b). Of the top 100 most abundant proteins
185 in the EVs, 65 have predicted transmembrane domains, whereas there are no such proteins among the top
186 100 most abundant cellular proteins. Thus, although Sis-EVs incorporate a considerable fraction of the total
187 *S. islandicus* proteome, there is a strong enrichment for certain functional categories and, in particular, for
188 membrane proteins. Presence in the Sis-EVs of proteins from nearly all functional categories suggests that
189 many of these proteins are incorporated non-selectively, by entrapment of the cytosolic and membrane
190 contents. It is possible that not all of the proteins are present within each Sis-EV, but are rather distributed
191 across the EV population.

192

193 *Sulfolobus* EVs have been previously shown to carry toxins, dubbed sulfolobocins, active against closely
194 related *Sulfolobus* species [63, 64]. However, homologs of these particular toxins are not encoded in the *S.*
195 *islandicus* REY15A genome. Nevertheless, nearly one third of proteins in the O category in Sis-EVs
196 corresponded to diverse proteases and nucleases. Notably, we also detected two putative toxins
197 (WP_014512538 and WP_014512541) of the RNase A family and several hydrolases of diverse
198 specificities (Fig. 2c; Supplementary Data 1). This finding suggested that deployment of the Sis-EV payload
199 could be toxic to recipient cells lacking necessary immunity. Incubation of Sis-EVs with *Sulfolobus* cells
200 for 3 h indeed resulted in modest, albeit significant, decrease in colony forming units for *S. solfataricus*
201 cells, but not for the more distantly related *S. acidocaldarius* or *S. shibatae* (Fig. S5a). However, the
202 inhibitory effect of Sis-EVs on *S. solfataricus* was temporary and was lifted when the incubation was
203 prolonged to 5 h (Fig. S5b). Thus, Sis-EVs do not appear to participate in intermicrobial conflicts, at least,
204 not among the tested *Sulfolobus* species.

205

206 Sis-EVs contained all six components of the *Sulfolobus* ESCRT machinery (arCOG category D; Fig. 2c),
207 consistent with the possibility that ESCRT machinery is involved in EV biogenesis [51]. Label-free
208 intensity-based absolute quantification (iBAQ) [65] of protein abundances showed that two of the ESCRT
209 components, ESCRT-III-2 and ESCRT-III-1, were among the top-10 most abundant proteins in Sis-EVs
210 (Fig. 2c). Western blot analysis has confirmed that both proteins were present and strongly enriched in Sis-
211 EVs (Fig. S6). As expected, both S-layer proteins were found in the EVs, with SlaA being the most abundant
212 protein in Sis-EVs (Fig. 2c).

213

214 **Sis-EVs carry plasmid and genomic DNA**

215 Sis-EVs carried the chromatin proteins Sac7d/Sso7d and Alba (Fig. 2c), responsible for compaction of the
216 *Sulfolobus* chromosome [66, 67], suggesting that Sis-EVs contain DNA. Indeed, DNA has been previously
217 observed in EVs from halophilic archaea and *Thermococcus* spp. (both in the phylum Euryarchaeota) [18,
218 19, 21, 68] but never reported in *Sulfolobus* EVs. To test if Sis-EVs carry DNA, purified EVs were treated
219 with DNase I and stained with 4',6-diamidino-2-phenylindole (DAPI). The DAPI-stained Sis-EVs could be
220 detected by both flow cytometry (Fig. 3a) and fluorescence microscopy (Fig. 3b), consistent with the
221 presence of DNA. Notably, only 13.3% of EVs detected by the flow cytometry were DAPI-positive,
222 whereas the majority of EVs were DAPI-negative, indicating a heterogeneity of the EV content.

223

224 High-throughput sequencing of the DNA extracted from Sis-EVs yielded reads aligning to both the *S.*
225 *islandicus* chromosome and the resident extrachromosomal plasmid pSeSD. Both replicons were covered
226 throughout their respective lengths (Fig. 3c), but the median sequencing depth of the plasmid was 19 times
227 higher than that of the chromosome (386× versus 20× coverage, respectively). This difference cannot be
228 explained by the higher copy number of the plasmid (3-5 copies per 1 chromosome copy) [69]. It is most
229 probable that, as in the case of the *Thermococcus* [70] and bacterial [8] EVs, overlapping genomic
230 fragments of variable sizes, rather than complete chromosome, are packed into the Sis-EVs.

231

232 To test the biological relevance of DNA incorporation into Sis-EVs, we investigated the ability of Sis-EVs
233 to transfer the plasmid-borne *pyrEF* locus into a plasmid-free auxotrophic strain E233S of *S. islandicus*
234 carrying a chromosomal deletion in the *pyrEF* operon responsible for uracil synthesis (Fig. S7) [69]. To
235 this end, Sis-EVs produced by the pSeSD-carrying strain were purified, treated with DNase I, incubated
236 with recipient E233S cells in liquid culture and plated on solid medium devoid of uracil. In the presence of
237 EVs, strain E233S formed over 1000-fold more colonies than the control E233S cells (Fig. 3d), whereas
238 plating of EVs alone did not yield colonies on either rich or uracil-deficient medium (Fig. S8a), further
239 confirming that there were no cells contaminating EV preparation. Approximately half of the colonies
240 obtained after incubation with Sis-EVs carried the pSeSD plasmid (Fig. S8b-e). To test if the plasmid-
241 devoid strains carry the *pyrEF* cassette elsewhere on the chromosome, we performed PCR with the *pyrF*-
242 specific primers (Fig. S7). However, *pyrF* gene was present exclusively in the pSeSD-carrying strains (Fig.
243 S8f), indicating that there was no ectopic *pyrF* integration. Next, we verified if the ability of the plasmid-
244 lacking strains to grow in the absence of uracil was inheritable. To this end, the plasmid-containing and
245 plasmid-deficient cells from initial colonies were resuspended in the selective medium and spotted on the
246 solid medium lacking uracil (Fig. S8g). Only plasmid-containing strains could grow, suggesting that initial
247 growth of the colonies in the absence of uracil was supported by the nutrients provided by the EVs, whereas
248 transfer of such colonies into fresh medium arrested the cell growth, unless the cells contained pSeSD.
249 Collectively, these results demonstrate that Sis-EVs carry DNA and act as vehicles for gene transfer. The
250 exact mechanism of EV-mediated gene transfer into recipient cells remains unclear but, presumably, it
251 involves fusion between the EV and cell membranes.

252

253 **Sis-EVs support heterotrophic growth of *Sulfolobus* cells**

254 To further investigate if EVs can provide nutrients (other than uracil) to support heterotrophic cell growth,
255 *Sulfolobus* cells were inoculated in media lacking nitrogen and/or carbon source. As expected, cells could
256 not grow in the medium containing only mineral salts and a mix of vitamins (Fig. 4a), nor could they grow

257 when only carbon source (sucrose) was added to this solution (Fig. 4b). Instead, slight decrease in optical
258 density of the culture was observed, suggesting partial lysis. However, when either medium was
259 supplemented with purified Sis-EVs, there was significant (two paired T-test, $p < 0.05$), Sis-EV
260 concentration-dependent increase in the optical density of *S. islandicus* culture, indicative of cell growth
261 (Fig. 4). The same result was obtained with EVs isolated from Sis/pSeSD-CdvA (see below). These results
262 strongly suggest that EVs can serve as a source of both carbon and nitrogen, and hence play an important
263 role in nutrient cycling in extreme environments. Similarly, it has been shown that EVs produced by
264 cyanobacteria can support the growth of heterotrophic bacteria by serving as a carbon source [7].
265

266 To the best of our knowledge, production of EVs by different Sulfolobales strains or by any other archaeal
267 strain has been reported only under laboratory cultivation conditions. To verify whether EVs are also
268 produced in the environment, we analyzed a previously collected archaea-dominated hot spring sample [71]
269 for the presence of EVs. The contents of the sample were directly concentrated by ultracentrifugation
270 without prior cultivation in the laboratory and visualized by TEM. We observed multiple S-layer-coated
271 EVs closely resembling those produced by Sulfolobales species (Fig. S9). The diameter of the observed
272 EVs varied between 77 and 182 nm, which is considerably smaller than the size of the smallest known
273 archaea, i.e., *Nanoarchaea* spp. with the diameter of ~400 nm [72, 73], confirming that these are subcellular
274 structures. These results strongly suggest that Sis-EVs are not laboratory artifacts and are environmentally
275 and biologically relevant.
276

277 **Sis-EVs biogenesis is ESCRT-dependent**

278 Sis-EV biogenesis occurs through budding from the cytoplasmic membrane (Fig. 5a) and ESCRT system
279 is a prime suspect implicated in membrane constriction and scission. To investigate the involvement of
280 ESCRT machinery in EV biogenesis, we constructed a collection of knockdown strains in which expression
281 of each of the six ESCRT machinery components was depleted by the endogenous type III-B CRISPR-Cas
282 system of *S. islandicus*. The utility of this strategy for gene knockdown has been recently demonstrated in
283 *Sulfolobus* [54, 74, 75]. Quantitative reverse transcription PCR (RT-qPCR) analysis has shown that whereas
284 expression of *escrt-III* was decreased by ~30%, expression of all other genes was down by 60-70% (Fig.
285 5b). Western blot analysis of *escrt-III-1* and *escrt-III-2* knockdown strains has shown that the levels of the
286 corresponding proteins have been decreased by 99% and 60%, respectively (Fig. S6b). It has been
287 previously shown that *escrt-III* and *vps4* are expressed from a bicistronic operon [44, 76] (Fig. S10a). Thus,
288 we verified whether CRISPR targeting of the *escrt-III* gene has a polar effect on the expression of the *vps4*.
289 There was no significant difference in the *vps4* transcript levels between the *escrt-III* knockdown and
290 control cells (Fig. S10b). This is consistent with the previous results showing that cleavage of a transcript
291 by type III-B CRISPR system in *S. islandicus* REY15A occurs within 20 bp of the CRISPR spacer targeting
292 [77]; that is, the fragment of the transcript encoding Vps4 is unaffected by the cleavage within the ESCRT-
293 III-encoding region (Fig. S10a).
294

295 Knockdown strains of *cdvA*, *vps4*, *escrt-III* and *escrt-III-1* displayed considerable cell growth defects,
296 whereas those of *escrt-III-2* and *escrt-III-3* showed nearly normal cell growth (Fig. S11a). The depletion of
297 *cdvA*, *vps4*, *escrt-III* and *escrt-III-1* transcripts by CRISPR targeting resulted in obvious cell division
298 defects (Fig. S11b, c), yielding cells 2-3 times larger than the control cells, and in slight increase (<7%) in
299 the fraction of dead cells in the corresponding populations (Fig. S11d). Consistent with the growth dynamics
300 (Fig. S11a), cell size of the *escrt-III-2* and *escrt-III-3* knockdown strains was similar to that of the control
301 cells (Fig. S11b and S11c). The lack of growth retardation for the *escrt-III-2* knockdown strain is somewhat
302 unexpected, given that all previous attempts to delete this gene in *S. islandicus* were unsuccessful, whereas
303 *escrt-III-3* is known to be non-essential for normal growth [38, 78]. Notably, under the growth conditions
304 used in this study, the expression of *escrt-III-3* was much lower than that of all other cell division genes
305 (Fig. S12). By contrast, the transcription level of *escrt-III-2* was six and three times higher than those of
306 *escrt-III* and *escrt-III-1*, respectively (Fig. S12). Thus, even with 60-70% decrease in transcript levels due
307 to CRISPR targeting, the total level of *escrt-III-2* transcripts would be comparable to that of other ESCRT-

308 III homologs. Presumably, these levels are sufficient for normal growth of *S. islandicus*. Notably, *escrt-III-*
309 *2* is not essential in *S. acidocaldarius* [40]. Thus, we do not exclude the possibility that *escrt-III-2* is also
310 not strictly required for the growth of *S. islandicus* and that previous attempts to delete this gene were
311 hindered by other factors.

312
313 Quantification of Sis-EVs produced by the knockdown strains has shown that whereas depletion of *cdvA*
314 had no significant effect on Sis-EV titer, all other knockdown strains, including the non-essential *escrt-III-*
315 *3*, produced significantly less EVs compared to the control strain (Fig. 5c). The *vps4* knockdown strain
316 displayed the strongest effect, with EV production being decreased by over 70%. Notably, it is possible that
317 different ESCRT-III homologs can partially complement each other during EV biogenesis. Interestingly,
318 overexpression of the ESCRT-III-1 and ESCRT-III-2 from a plasmid resulted in 200-250% increase in
319 vesiculation (Fig. 5d) consistent with their role in Sis-EV budding. Unexpectedly, overexpression of CdvA
320 resulted in hypervesiculation phenotype (Fig. 5d). However, the same effect was also observed when CdvA
321 lacking the C-terminal domain (CdvA Δ C) responsible for interaction with ESCRT-III [43, 44] was
322 overexpressed (Fig. S13a), suggesting that excessive binding of CdvA to the membrane [44] precipitates
323 the observed phenomenon. Overexpression of *cdvA* and *cdvA Δ C* yielded cells with up to 2-5 fold larger
324 diameters (Fig. S13b). By contrast, overexpression of ESCRT-III-1 and ESCRT-III-2 had no effect on cell
325 size or cell viability (Fig. S13b and S13c). Taken together, the overexpression and knockdown results show
326 that there is no apparent link between the cell size and EV biogenesis.

327
328 Budding of EVs from the control and overexpression strains was observed directly by TEM (Fig. 5a).
329 Notably, EVs produced by the CdvA overexpression strain were considerably larger than those from the
330 control (Fig. 1a) and ESCRT-III-2 overexpression (Fig. 5e) strains, with an average diameter of 235 nm
331 versus 177 and 181 nm, respectively (Fig. 1b and 5f). To exclude the possibility that the large EVs produced
332 by the CdvA overexpression strain represent small cells, the EV-containing supernatant was filtered through
333 0.45 μ m filter and plated on the solid medium. No colonies were formed (Fig. S4b). Our results strongly
334 suggest that EV budding in *Sulfolobus* is dependent on the ESCRT machinery, including Vps4 ATPase and
335 the ESCRT-III ensemble, whereas CdvA appears to be dispensable for this process.

336 337 **Sis-EVs biogenesis is linked to cell division**

338 The expression of ESCRT-III homologs in *S. acidocaldarius* is linked to the cell cycle [37, 79]. To verify
339 whether the same is true for *S. islandicus* and if EV biogenesis is linked to the cell cycle, we synchronized
340 the *S. islandicus* culture by adapting a protocol previously used for *S. acidocaldarius* [79, 80]. The cells were
341 arrested at the G2 phase using acetic acid and could progress into cell division phase following the removal
342 of the acid (see Materials and Methods for details). Analysis of the DNA content by flow cytometry has
343 shown that the cells started transitioning from G2 into the cell division phase at 90 min following the
344 removal of the acetic acid (Fig. 6a). Western blot analysis of the synchronized cells has shown that ESCRT-
345 III, ESCRT-III-1 and ESCRT-III-2 proteins were undetectable during the G2 phase and became detectable
346 at 90 min after the removal of acetic acid (Fig. 6b). Notably, however, whereas ESCRT-III was abundantly
347 expressed at this time point, ESCRT-III-1 and ESCRT-III-2 were barely detectable. Conversely, at 150 min
348 time point, when the expression of ESCRT-III-1 and ESCRT-III-2 peaked, the expression of ESCRT-III
349 started to decline (Fig. 6b). This dynamics is consistent with the recent suggestion that ESCRT-III is the
350 first to form a ring in the mid-cell during cell division, which serves a platform for subsequent recruitment
351 of ESCRT-III-1 and ESCRT-III-2 [79]. We next analyzed the production of Sis-EVs in synchronized
352 cultures at 60 (G2 phase), 90 (beginning of cell division) and 135 (advanced cell division) min after removal
353 of acetic acid (Fig. 6c). There was a dramatic increase in EV production at the 135 min time point which
354 coincides with active cell division (Fig. 6c, Fig. S14). These results strongly suggest that Sis-EV production
355 is linked to the cell division and might be triggered by the natural, cell cycle-linked changes in the
356 expression of ESCRT-III homologs. In particular, the active EV production appears to coincide with the
357 expression pattern of ESCRT-III-1 and ESCRT-III-2, rather than ESCRT-III, suggesting a prime role of
358 these proteins in EV budding. This conclusion is fully consistent with the observation that the two proteins

359 are strongly enriched in EVs as well as with the fact that overexpression of ESCRT-III-1 and ESCRT-III-
360 2, but not ESCRT-III, induces EV biogenesis.

361

362 **CONCLUDING REMARKS**

363 Here we have further characterized *Sulfolobus* EVs and showed that they carry DNA. Combined with the
364 previous observation of DNA-containing EVs in euryarchaea (halobacteria and thermococci) [18, 19, 21,
365 52, 68, 81, 82], the finding that crenarchaeal EVs also contain DNA suggests that this property might be
366 general across archaea. Horizontal gene transfer (HGT) is essential for the survival of microbial populations
367 that otherwise deteriorate due to the Muller's ratchet [83, 84]. Some bacteria and archaea are naturally
368 competent and can uptake DNA from the environment [85, 86]. However, in low-density populations
369 residing in high-temperature, acidic environments, as is the case for Sulfolobales, extracellular DNA might
370 be neither stable nor readily available. In bacteria, conjugative plasmids, transducing bacteriophages and
371 phage-derived gene transfer agents are considered the main drivers of the HGT. Although conjugative
372 plasmids are known in *Sulfolobus*, their role in HGT has not been assessed [87]. By contrast, transducing
373 viruses or dedicated gene transfer agents have not been described in Sulfolobales. Full-length genomic
374 DNA could not be detected in the agarose gel, suggesting that only fragments of genomic DNA, which
375 could represent byproducts of genome replication and repair, are incorporated into the Sis-EVs.
376 Nevertheless, these DNA fragments collectively represented all genes present on the *S. islandicus*
377 chromosome, as well as the resident plasmid. Importantly, Sis-EVs could successfully transfer the marker
378 genes as well as the complete plasmid within the *S. islandicus* population. Furthermore, our data shows that
379 *S. islandicus* can use EVs as carbon and nitrogen source, which is likely to be important in natural settings
380 where nutrients are scarce. Collectively, these results indicate that EVs could play an important, yet
381 overlooked role in gene transfer and nutrient flux in extreme environments. Indeed, we observed EVs
382 resembling those produced by Sulfolobales directly in the environmental archaea-dominated sample,
383 suggesting that properties of the EVs determined under laboratory conditions are biologically and
384 environmentally relevant.

385

386 The mechanisms of EV biogenesis are poorly understood in prokaryotes [1]. Our results strongly suggest
387 that *Sulfolobus* ESCRT machinery plays an important role in EVs formation. Importantly, EV budding
388 appears to be specifically linked to cell division, when the expression of the ESCRT-III proteins is the
389 highest. By contrast, CdvA appears to be dispensable for EV budding suggesting that there are mechanistic
390 differences of the archaeal ESCRT functioning in different pathways of membrane remodeling. This would
391 be similar to eukaryotes, where ESCRT-III complex is targeted to the membranes by different partner
392 proteins [22]. We hypothesize that CdvA is substituted by a different targeting protein during EV budding.
393 Notably, some archaea lack *cdvA* gene but encode ESCRT-III and Vps4 homologs [31, 45-47], suggesting
394 that ESCRT-III targeting to the membrane in these organisms, similar to eukaryotes, is achieved by an
395 unrelated protein or proteins. Alternatively, changes in membrane curvature at the EV budding sites might
396 promote binding of ESCRT-III paralogs, without the necessary chaperoning of CdvA. Further in vitro
397 experiments will be necessary to test this hypothesis. Regardless, our results show that the ESCRT-
398 dependent mechanism of EV biogenesis is conserved in both archaea and eukaryotes, and likely represents
399 one of the ancestral functions of the ESCRT system.

400 **MATERIALS AND METHODS**

401 **Strains, growth conditions and transformation of *Sulfolobus***

402 *Sulfolobus islandicus* strains REY15A and E233S (REY15A Δ pyrEF Δ lacS) [69], and *Sulfolobus*
403 *solfatarius* PH1-16 (PH1 pyrF mutant) [88], hereafter PH1-16, were grown aerobically with shaking (145
404 rpm) at 75°C in 30 ml of STVU medium containing mineral salts (M), 0.2% (wt/vol) sucrose (S), 0.2%
405 (wt/vol) tryptone (T), a mixed vitamin solution (V) and 0.01% (wt/vol) uracil (U); the pH was adjusted to
406 3.5 with sulfuric acid, as described previously [69]. SCV medium containing 0.2% (wt/vol) casamino acids
407 (C) was used for selection of uracil prototrophic transformants. ATV medium containing 0.2% (wt/vol)
408 arabinose (A) was used to induce protein overexpression and RNA interference. The plasmids and strains
409 constructed and used in this study are listed in Tables S2 and S3, respectively. *S. islandicus* cells were
410 synchronized using acetic acid (final concentration, 6 mM) as previously described for *S. acidocaldarius*
411 [79, 80] (see Supplementary Methods for further details).

412

413 **Isolation and purification of EVs**

414 EVs were isolated from liquid cultures of *S. islandicus* E233S or *S. solfataricus* PH1-16 strains carrying
415 shuttle vector pSeSD. The cells were grown at 75°C in appropriate medium and EVs were harvested at the
416 indicated times. Cells were removed by centrifugation at 7,000 rpm at 4°C for 20 min. The supernatant was
417 filtered with 0.45 μ m filter and EVs collected by ultracentrifugation at 40,000 rpm (Type 45 Ti rotor) at
418 4°C for 2 h, followed by 100,000 rpm (TLA 100.2 rotor) at 4°C for 1 h, and then re-suspended in 500 μ l of
419 PBS.

420

421 For mass spectrometry (see Supplementary Methods) and DNA content sequencing, the EVs were collected
422 during the exponential growth phase (24 h) and further purified by ultracentrifugation in sucrose gradient
423 (50%, 45%, 40%, 35%, 30%, and 25%) at 25,000 rpm (SW 60 rotor) at 4°C for 10 min. The EVs formed
424 an opalescent band in the region of the gradient corresponding to 30-40% sucrose (Fig. S15). The band was
425 collected and EVs pelleted by ultracentrifugation at 100,000 rpm (TLA100.2 rotor) at 4°C for 1 h. The
426 resulting pellet was re-suspended in 500 μ l of PBS.

427

428 **Transmission electron microscopy**

429 For TEM analysis, EVs or cell cultures were absorbed to glow-discharged copper grids with carbon-coated
430 Formvar film and negatively stained with 2.0% (w/v) uranyl acetate. The samples were observed under FEI
431 Tecnai Spirit BioTwin 120 microscope (FEI, Eindhoven, The Netherlands) operated at 120 kV.

432

433 **Flow cytometry and quantification of EVs**

434 EVs were isolated from 50 ml cultures of E233S and PH1-16 cells carrying pSeSD vector at the given time
435 points of cell growth, then 50 μ l of the EV preparations were mixed with 250 μ l PBS staining buffer
436 containing 2.5 μ g/ml DAPI (4', 6-diamidino-2-phenylindole; Thermo Fisher Scientific, USA) and kept at
437 4°C for 30 min. The EVs were analyzed and sorted on the MoFlo Astrios cell sorter (Beckman Coulter)
438 equipped with an EQ module specifically developed to detect nanoparticles and with 488 nm and 561 nm
439 lasers at 200 mW. The calibration of the machine was carried out using FITC-labelled Megamix-Plus SSC
440 beads from BioCytex (Fig. S1). The sheath-liquid 0.9% NaCl (Revol, France) was filtered through a 0.04
441 μ m filter. The analysis was performed using the side-scattered (SSC) light parameter of laser 561, with
442 threshold set to 0.012% in order to have maximum of 300 events per second. An M2 mask was added in
443 front of the forward-scattered (FSC) light.

444

445 To count the EVs, we used Trucount™ Tubes (BD Biosciences, San Diego, CA), which contain a defined
446 number of fluorescently labeled beads and have been specifically designed for reproducible counting of
447 various biological nanoparticles, including EVs [89, 90]. For quantification, we added the same volume
448 (300 μ l) of EV preparations into the tubes that contained the constant number of beads. The EV number
449 was calculated using the following formula: $EV_{total} = (EV \text{ count}/\text{bead count}) \times \text{total number of beads in the}$
450 $\text{Trucount}^{\text{TM}}$ Tube. In each case, the samples were passed through the flow cytometer's detector until 2000

451 beads were recorded. All quantifications by flow cytometry were done in triplicate (Fig. S14 and Fig. S16).
452 Further details on cell cycle and cell size analysis by flow cytometry can be found in Supplementary
453 Methods.

454

455 **DNA isolation from EVs and sequencing**

456 To remove the traces of extravesicular nucleic acids, prior to DNA extraction, EVs were incubated with
457 DNase I (15 U/ml) and RNase (100 µg/ml), in the presence of MgCl₂ (10 mM), at 37°C for 30 min, followed
458 by addition of EDTA (20 mM). EVs were disrupted by proteinase K (100 µg/ml) and SDS (0.5%) treatment
459 at 55°C for 30 min. The DNA was extracted by standard phenol/chloroform procedure, precipitated with
460 0.3 M sodium acetate (pH 5.3) and isopropanol. The resultant pellet was resuspended in DNase/RNase-free
461 water and used for sequencing. Sequencing libraries were prepared from 100 ng of DNA with the TruSeq
462 DNA PCR-Free library Prep Kit from Illumina and sequenced on Illumina MiSeq platform with 150-bp
463 paired-end read lengths (Institut Pasteur, France). Raw sequence reads were processed with Trimmomatic
464 v.0.3.6 and mapped to the reference genomes of REY15A and pSeSD plasmid using Bowtie2 [91] with
465 default parameters and analyzed with Sequana [92].

466

467 **EV-mediated gene transfer**

468 EVs isolated and purified from 6 L of exponentially growing Sis/pSeSD culture (24 h) were used for gene
469 transfer experiments as described previously [93], with some modification (see Supplementary Methods).

470

471 **Live/Dead staining and fluorescence microscopy analysis**

472 Live/Dead staining was carried out using the LIVE/DEAD *BacLight*TM Bacterial Viability Kit (Invitrogen,
473 US) [94, 95] according to the supplier's protocols. See Supplementary Methods for the detailed protocol.

474

475 **Overexpression of ESCRT proteins**

476 Plasmids expressing different ESCRT machinery components and their mutants were described previously
477 [38] (Table S2). Briefly, cells harboring the plasmids were first inoculated into 30 ml of the MTSV medium
478 and when the OD₆₀₀ reached ~0.6-0.8, they were transferred into the ATV medium containing 0.2% (wt/vol)
479 arabinose with an initial OD₆₀₀ of 0.05 to induce protein expression. All plasmids are listed in Table S3.

480

481 **Construction of the CRISPR type III-B-based RNA interference plasmids and RNA interference**

482 The CRISPR type III-B-based RNA interference plasmids were constructed according to the methods
483 described previously [74, 77]. The spacers selected and used in this study are listed in Table S4, whereas
484 all other oligonucleotides are listed in Table S5. See Supplementary Methods for further details.

485

486 **Western blot**

487 ESCRT proteins were detected using antibodies against ESCRT-III, ESCRT-III-1 and ESCRT-III-2
488 (HuaAn Biotechnology Co., Hangzhou, Zhejiang, China), as described previously [38]. See Supplementary
489 Methods for further details.

490 **ACKNOWLEDGEMENTS**

491 This work was supported by l'Agence Nationale de la Recherche (#ANR-17-CE15-0005-01) and Ville de
492 Paris Emergence(s) program (project MEMREMA) grants to M.K., and European Research Council grant
493 from the European Union's Seventh Framework Program (FP/2007-2013)/Project EVOMOBIL-ERC Grant
494 Agreement 340440 to P.F. J.L. was partly supported through the PRESTIGE post-doctoral program from
495 European Union's Seventh Framework Programme, the National Key Research and Development Program
496 of China (No. 2020YFA0906800), and the post-doctoral fellowship from the State Key Laboratory of
497 Microbial Technology, Shandong University. The authors would like to thank Thibault Chaze and Mariette
498 Matondo (Proteomics Platform, Institut Pasteur) as well as Thomas Cokelaer and Marc Monot (Biomics
499 Platform, Institut Pasteur) for help with the proteomics and sequencing analyses, respectively. We are also
500 grateful to the Ultrastructural BioImaging (UTechS UBI) unit of Institut Pasteur for access to electron
501 microscopes. We gratefully acknowledge the UtechS Photonic BioImaging (Imagopole), C2RT, Institut
502 Pasteur, supported by the French National Research Agency (France BioImaging; ANR-10-INSB-04;
503 Investments for the Future).

504

505 **CONFLICT OF INTEREST**

506 The authors declare that they have no conflict of interest.

507 **REFERENCES**

- 508 1. Coelho C, Casadevall A. Answers to naysayers regarding microbial extracellular vesicles. *Biochem Soc*
509 *Trans.* 2019; 47:1005-1012.
- 510 2. Woith E, Fuhrmann G, Melzig MF. Extracellular vesicles-connecting kingdoms. *Int J Mol Sci.* 2019;
511 20:E5695.
- 512 3. Gill S, Catchpole R, Forterre P. Extracellular membrane vesicles in the three domains of life and beyond.
513 *FEMS Microbiol Rev.* 2019; 43:273-303.
- 514 4. Brown L, Wolf JM, Prados-Rosales R, Casadevall A. Through the wall: extracellular vesicles in Gram-
515 positive bacteria, mycobacteria and fungi. *Nat Rev Microbiol.* 2015; 13:620-30.
- 516 5. Schatz D, Vardi A. Extracellular vesicles - new players in cell-cell communication in aquatic
517 environments. *Curr Opin Microbiol.* 2018; 43:148-154.
- 518 6. Soler N, Krupovic M, Marguet E, Forterre P. Membrane vesicles in natural environments: a major
519 challenge in viral ecology. *ISME J.* 2015; 9:793-6.
- 520 7. Biller SJ, Schubotz F, Roggensack SE, Thompson AW, Summons RE, Chisholm SW. Bacterial vesicles in
521 marine ecosystems. *Science.* 2014; 343:183-6.
- 522 8. Biller SJ, McDaniel LD, Breitbart M, Rogers E, Paul JH, Chisholm SW. Membrane vesicles in sea water:
523 heterogeneous DNA content and implications for viral abundance estimates. *ISME J.* 2017; 11:394-404.
- 524 9. Denham J, Spencer SJ. Emerging roles of extracellular vesicles in the intercellular communication for
525 exercise-induced adaptations. *Am J Physiol Endocrinol Metab.* 2020.
- 526 10. Abramowicz A, Story MD. The long and short of it: The emerging roles of non-coding RNA in small
527 extracellular vesicles. *Cancers (Basel).* 2020; 12.
- 528 11. Ghossein YS, Lee J. Special issue on the role of extracellular vesicles in human diseases. *Exp Mol Med.* 2019;
529 51:34.
- 530 12. Mallocci M, Perdomo L, Veerasamy M, Andriantsitohaina R, Simard G, Martinez MC. Extracellular
531 vesicles: Mechanisms in human health and disease. *Antioxid Redox Signal.* 2019; 30:813-856.
- 532 13. Linxweiler J, Junker K. Extracellular vesicles in urological malignancies: an update. *Nat Rev Urol.* 2020;
533 17:11-27.
- 534 14. Xu R, Rai A, Chen M, Suwakulsiri W, Greening DW, Simpson RJ. Extracellular vesicles in cancer -
535 implications for future improvements in cancer care. *Nat Rev Clin Oncol.* 2018; 15:617-638.
- 536 15. Ramasubramanian L, Kumar P, Wang A. Engineering extracellular vesicles as nanotherapeutics for
537 regenerative medicine. *Biomolecules.* 2019; 10.
- 538 16. Villa F, Quarto R, Tasso R. Extracellular vesicles as natural, safe and efficient drug delivery systems.
539 *Pharmaceutics.* 2019; 11.
- 540 17. Gorlas A, Marguet E, Gill S, Geslin C, Guigner JM, Guyot F *et al.* Sulfur vesicles from Thermococcales:
541 A possible role in sulfur detoxifying mechanisms. *Biochimie.* 2015; 118:356-64.
- 542 18. Erdmann S, Tschitschko B, Zhong L, Raftery MJ, Cavicchioli R. A plasmid from an Antarctic haloarchaeon
543 uses specialized membrane vesicles to disseminate and infect plasmid-free cells. *Nat Microbiol.* 2017;
544 2:1446-1455.
- 545 19. Gaudin M, Krupovic M, Marguet E, Gaudiard E, Cvirkaite-Krupovic V, Le Cam E *et al.* Extracellular
546 membrane vesicles harbouring viral genomes. *Environ Microbiol.* 2014; 16:1167-75.
- 547 20. Soler N, Gaudin M, Marguet E, Forterre P. Plasmids, viruses and virus-like membrane vesicles from
548 Thermococcales. *Biochem Soc Trans.* 2011; 39:36-44.
- 549 21. Choi DH, Kwon YM, Chiura HX, Yang EC, Bae SS, Kang SG *et al.* Extracellular vesicles of the
550 hyperthermophilic archaeon *Thermococcus onnurineus* NA1T. *Appl Environ Microbiol.* 2015; 81:4591-
551 9.
- 552 22. Vietri M, Radulovic M, Stenmark H. The many functions of ESCRTs. *Nat Rev Mol Cell Biol.* 2020; 21:25-
553 42.

554 23. Juan T, Furthauer M. Biogenesis and function of ESCRT-dependent extracellular vesicles. *Semin Cell*
555 *Dev Biol.* 2018; 74:66-77.

556 24. van Niel G, D'Angelo G, Raposo G. Shedding light on the cell biology of extracellular vesicles. *Nat Rev*
557 *Mol Cell Biol.* 2018; 19:213-228.

558 25. Christ L, Raiborg C, Wenzel EM, Campsteijn C, Stenmark H. Cellular functions and molecular
559 mechanisms of the ESCRT membrane-scission machinery. *Trends Biochem Sci.* 2017; 42:42-56.

560 26. Schöneberg J, Lee IH, Iwasa JH, Hurley JH. Reverse-topology membrane scission by the ESCRT proteins.
561 *Nat Rev Mol Cell Biol.* 2017; 18:5-17.

562 27. Hurley JH. ESCRTs are everywhere. *Embo J.* 2015; 34:2398-407.

563 28. Mierzwa BE, Chiaruttini N, Redondo-Morata L, von Filseck JM, König J, Larios J *et al.* Dynamic subunit
564 turnover in ESCRT-III assemblies is regulated by Vps4 to mediate membrane remodelling during
565 cytokinesis. *Nat Cell Biol.* 2017; 19:787-798.

566 29. Adell MA, Vogel GF, Pakdel M, Müller M, Lindner H, Hess MW *et al.* Coordinated binding of Vps4 to
567 ESCRT-III drives membrane neck constriction during MVB vesicle formation. *J Cell Biol.* 2014; 205:33-
568 49.

569 30. Samson RY, Dobro MJ, Jensen GJ, Bell SD. The structure, function and roles of the archaeal ESCRT
570 apparatus. *Subcell Biochem.* 2017; 84:357-377.

571 31. Zaremba-Niedzwiedzka K, Cáceres EF, Saw JH, Backstrom D, Juzokaite L, Vancaester E *et al.* Asgard
572 archaea illuminate the origin of eukaryotic cellular complexity. *Nature.* 2017; 541:353-358.

573 32. Makarova KS, Yutin N, Bell SD, Koonin EV. Evolution of diverse cell division and vesicle formation
574 systems in Archaea. *Nat Rev Microbiol.* 2010; 8:731-41.

575 33. Lindås AC, Karlsson EA, Lindgren MT, Ettema TJ, Bernander R. A unique cell division machinery in the
576 Archaea. *Proc Natl Acad Sci U S A.* 2008; 105:18942-6.

577 34. Lu Z, Fu T, Li T, Liu Y, Zhang S, Li J *et al.* Coevolution of eukaryote-like Vps4 and ESCRT-III subunits in
578 the Asgard archaea. *mBio.* 2020; 11:e00417-20.

579 35. Ng KH, Srinivas V, Srinivasan R, Balasubramanian M. The *Nitrosopumilus maritimus* CdvB, but not FtsZ,
580 assembles into polymers. *Archaea.* 2013; 2013:104147.

581 36. Pelve EA, Lindas AC, Martens-Habbena W, de la Torre JR, Stahl DA, Bernander R. Cdv-based cell division
582 and cell cycle organization in the thaumarchaeon *Nitrosopumilus maritimus*. *Mol Microbiol.* 2011;
583 82:555-66.

584 37. Samson RY, Obita T, Freund SM, Williams RL, Bell SD. A role for the ESCRT system in cell division in
585 archaea. *Science.* 2008; 322:1710-3.

586 38. Liu J, Gao R, Li C, Ni J, Yang Z, Zhang Q *et al.* Functional assignment of multiple ESCRT-III homologs in
587 cell division and budding in *Sulfolobus islandicus*. *Mol Microbiol.* 2017; 105:540-553.

588 39. Yang N, Driessen AJ. Deletion of *cdvB* paralogous genes of *Sulfolobus acidocaldarius* impairs cell
589 division. *Extremophiles.* 2014; 18:331-9.

590 40. Pulschen AA, Mutavchiev DR, Culley S, Sebastian KN, Roubinet J, Roubinet M *et al.* Live imaging of a
591 hyperthermophilic archaeon reveals distinct roles for two ESCRT-III homologs in ensuring a robust and
592 symmetric division. *Curr Biol.* 2020.

593 41. Dobro MJ, Samson RY, Yu Z, McCullough J, Ding HJ, Chong PL *et al.* Electron cryotomography of ESCRT
594 assemblies and dividing *Sulfolobus* cells suggests that spiraling filaments are involved in membrane
595 scission. *Mol Biol Cell.* 2013; 24:2319-27.

596 42. Samson RY, Duggin IG, Bell SD. Analysis of the archaeal ESCRT apparatus. *Methods Mol Biol.* 2019;
597 1998:1-11.

598 43. Moriscot C, Gribaldo S, Jault JM, Krupovic M, Arnaud J, Jamin M *et al.* Crenarchaeal CdvA forms double-
599 helical filaments containing DNA and interacts with ESCRT-III-like CdvB. *PLoS One.* 2011; 6:e21921.

600 44. Samson RY, Obita T, Hodgson B, Shaw MK, Chong PL, Williams RL *et al.* Molecular and structural basis
601 of ESCRT-III recruitment to membranes during archaeal cell division. *Mol Cell.* 2011; 41:186-96.

- 602 45. Caspi Y, Dekker C. Dividing the archaeal way: The ancient Cdv cell-division machinery. *Front Microbiol.*
603 2018; 9:174.
- 604 46. Abby SS, Melcher M, Kerou M, Krupovic M, Stieglmeier M, Rossel C *et al.* *Candidatus Nitrosocaldus*
605 *cavascurensis*, an ammonia oxidizing, extremely thermophilic archaeon with a highly mobile genome.
606 *Front Microbiol.* 2018; 9:28.
- 607 47. Nunoura T, Takaki Y, Kakuta J, Nishi S, Sugahara J, Kazama H *et al.* Insights into the evolution of Archaea
608 and eukaryotic protein modifier systems revealed by the genome of a novel archaeal group. *Nucleic*
609 *Acids Res.* 2011; 39:3204-23.
- 610 48. Liu J, Cvirkaite-Krupovic V, Baquero DP, Yang Y, Zhang Q, Shen Y *et al.* Virus-induced cell gigantism and
611 asymmetric cell division in archaea. *Proc Natl Acad Sci U S A.* 2021; 118:e2022578118.
- 612 49. Snyder JC, Samson RY, Brumfield SK, Bell SD, Young MJ. Functional interplay between a virus and the
613 ESCRT machinery in archaea. *Proc Natl Acad Sci U S A.* 2013; 110:10783-7.
- 614 50. Quemin ER, Chlanda P, Sachse M, Forterre P, Prangishvili D, Krupovic M. Eukaryotic-like virus budding
615 in Archaea. *mBio.* 2016; 7:e01439-16.
- 616 51. Ellen AF, Albers SV, Huibers W, Pitcher A, Hobel CF, Schwarz H *et al.* Proteomic analysis of secreted
617 membrane vesicles of archaeal *Sulfolobus* species reveals the presence of endosome sorting complex
618 components. *Extremophiles.* 2009; 13:67-79.
- 619 52. Marguet E, Gaudin M, Gaudiard E, Fourquaux I, le Blond du Plouy S, Matsui I *et al.* Membrane vesicles,
620 nanopods and/or nanotubes produced by hyperthermophilic archaea of the genus *Thermococcus*.
621 *Biochem Soc Trans.* 2013; 41:436-42.
- 622 53. Zhang C, Wipfler RL, Li Y, Wang Z, Hallett EN, Whitaker RJ. Cell structure changes in the
623 hyperthermophilic crenarchaeon *Sulfolobus islandicus* lacking the S-layer. *mBio.* 2019; 10:e01589-19.
- 624 54. Zink IA, Pfeifer K, Wimmer E, Sleytr UB, Schuster B, Schleper C. CRISPR-mediated gene silencing reveals
625 involvement of the archaeal S-layer in cell division and virus infection. *Nat Commun.* 2019; 10:4797.
- 626 55. Peng N, Han W, Li Y, Liang Y, She Q. Genetic technologies for extremely thermophilic microorganisms
627 of *Sulfolobus*, the only genetically tractable genus of crenarchaea. *Sci China Life Sci.* 2017; 60:370-385.
- 628 56. Morales-Aparicio JC, Lara Vasquez P, Mishra S, Barran-Berdon AL, Kamat M, Basso KB *et al.* The impacts
629 of sortase A and the 4¹-phosphopantetheinyl transferase homolog Sfp on *Streptococcus mutans*
630 extracellular membrane vesicle biogenesis. *Front Microbiol.* 2020; 11:570219.
- 631 57. Rodvalho VR, da Luz BSR, Rabah H, do Carmo FLR, Folador EL, Nicolas A *et al.* Extracellular vesicles
632 produced by the probiotic *Propionibacterium freudenreichii* CIRM-BIA 129 mitigate inflammation by
633 modulating the NF-kappaB pathway. *Front Microbiol.* 2020; 11:1544.
- 634 58. Tartaglia NR, Nicolas A, Rodvalho VR, Luz B, Briard-Bion V, Krupova Z *et al.* Extracellular vesicles
635 produced by human and animal *Staphylococcus aureus* strains share a highly conserved core proteome.
636 *Sci Rep.* 2020; 10:8467.
- 637 59. Zwarycz AS, Livingstone PG, Whitworth DE. Within-species variation in OMV cargo proteins: the
638 *Myxococcus xanthus* OMV pan-proteome. *Mol Omics.* 2020; 16:387-397.
- 639 60. Makarova KS, Wolf YI, Koonin EV. Archaeal Clusters of Orthologous Genes (arCOGs): An update and
640 application for analysis of shared features between Thermococcales, Methanococcales, and
641 Methanobacteriales. *Life (Basel).* 2015; 5:818-40.
- 642 61. Vorontsov EA, Rensen E, Prangishvili D, Krupovic M, Chamot-Rooke J. Abundant lysine methylation
643 and N-terminal acetylation in *Sulfolobus islandicus* revealed by bottom-up and top-down proteomics.
644 *Mol Cell Proteomics.* 2016; 15:3388-3404.
- 645 62. Chu Y, Zhu Y, Chen Y, Li W, Zhang Z, Liu D *et al.* aKMT catalyzes extensive protein lysine methylation in
646 the hyperthermophilic archaeon *Sulfolobus islandicus* but is dispensable for the growth of the
647 organism. *Mol Cell Proteomics.* 2016; 15:2908-23.
- 648 63. Ellen AF, Rohulya OV, Fusetti F, Wagner M, Albers SV, Driessen AJ. The sulfolobacin genes of *Sulfolobus*
649 *acidocaldarius* encode novel antimicrobial proteins. *J Bacteriol.* 2011; 193:4380-7.

650 64. Prangishvili D, Holz I, Stieger E, Nickell S, Kristjansson JK, Zillig W. Sulfolobins, specific proteinaceous
651 toxins produced by strains of the extremely thermophilic archaeal genus *Sulfolobus*. *J Bacteriol.* 2000;
652 182:2985-8.

653 65. Schwanhausser B, Busse D, Li N, Dittmar G, Schuchhardt J, Wolf J *et al.* Global quantification of
654 mammalian gene expression control. *Nature.* 2011; 473:337-42.

655 66. Zhang Z, Guo L, Huang L. Archaeal chromatin proteins. *Sci China Life Sci.* 2012; 55:377-85.

656 67. White MF, Bell SD. Holding it together: chromatin in the Archaea. *Trends Genet.* 2002; 18:621-6.

657 68. Forterre P, Soler N, Krupovic M, Marguet E, Ackermann HW. Fake virus particles generated by
658 fluorescence microscopy. *Trends Microbiol.* 2013; 21:1-5.

659 69. Deng L, Zhu H, Chen Z, Liang YX, She Q. Unmarked gene deletion and host-vector system for the
660 hyperthermophilic crenarchaeon *Sulfolobus islandicus*. *Extremophiles.* 2009; 13:735-46.

661 70. Gaudin M, Gauliard E, Schouten S, Houel-Renault L, Lenormand P, Marguet E *et al.* Hyperthermophilic
662 archaea produce membrane vesicles that can transfer DNA. *Environ Microbiol Rep.* 2013; 5:109-16.

663 71. Baquero DP, Contursi P, Piochi M, Bartolucci S, Liu Y, Cvirkaite-Krupovic V *et al.* New virus isolates from
664 Italian hydrothermal environments underscore the biogeographic pattern in archaeal virus
665 communities. *ISME J.* 2020; 14:1821-1833.

666 72. Hamm JN, Erdmann S, Eloe-Fadrosh EA, Angeloni A, Zhong L, Brownlee C *et al.* Unexpected host
667 dependency of Antarctic Nanohaloarchaeota. *Proc Natl Acad Sci U S A.* 2019; 116:14661-14670.

668 73. Huber H, Hohn MJ, Rachel R, Fuchs T, Wimmer VC, Stetter KO. A new phylum of Archaea represented
669 by a nanosized hyperthermophilic symbiont. *Nature.* 2002; 417:63-7.

670 74. Li Y, Pan S, Zhang Y, Ren M, Feng M, Peng N *et al.* Harnessing Type I and Type III CRISPR-Cas systems
671 for genome editing. *Nucleic Acids Res.* 2016; 44:e34.

672 75. Zebec Z, Manica A, Zhang J, White MF, Schleper C. CRISPR-mediated targeted mRNA degradation in
673 the archaeon *Sulfolobus solfataricus*. *Nucleic Acids Res.* 2014; 42:5280-8.

674 76. Wurtzel O, Sapra R, Chen F, Zhu Y, Simmons BA, Sorek R. A single-base resolution map of an archaeal
675 transcriptome. *Genome Res.* 2010; 20:133-41.

676 77. Peng W, Feng M, Feng X, Liang YX, She Q. An archaeal CRISPR type III-B system exhibiting distinctive
677 RNA targeting features and mediating dual RNA and DNA interference. *Nucleic Acids Res.* 2015; 43:406-
678 17.

679 78. Zhang C, Phillips APR, Wipfler RL, Olsen GJ, Whitaker RJ. The essential genome of the crenarchaeal
680 model *Sulfolobus islandicus*. *Nat Commun.* 2018; 9:4908.

681 79. Tarrason Risa G, Hurtig F, Bray S, Hafner AE, Harker-Kirschneck L, Faull P *et al.* The proteasome controls
682 ESCRT-III-mediated cell division in an archaeon. *Science.* 2020; 369.

683 80. Lundgren M, Andersson A, Chen L, Nilsson P, Bernander R. Three replication origins in *Sulfolobus*
684 species: synchronous initiation of chromosome replication and asynchronous termination. *Proc Natl*
685 *Acad Sci U S A.* 2004; 101:7046-51.

686 81. Soler N, Forterre P. Vesiduction: the fourth way of HGT. *Environ Microbiol.* 2020; 22:2457-2460.

687 82. Soler N, Marguet E, Verbavatz JM, Forterre P. Virus-like vesicles and extracellular DNA produced by
688 hyperthermophilic archaea of the order Thermococcales. *Res Microbiol.* 2008; 159:390-9.

689 83. Koonin EV. Horizontal gene transfer: essentiality and evolvability in prokaryotes, and roles in
690 evolutionary transitions. *F1000Res.* 2016; 5.

691 84. Takeuchi N, Kaneko K, Koonin EV. Horizontal gene transfer can rescue prokaryotes from Muller's
692 ratchet: benefit of DNA from dead cells and population subdivision. *G3 (Bethesda).* 2014; 4:325-39.

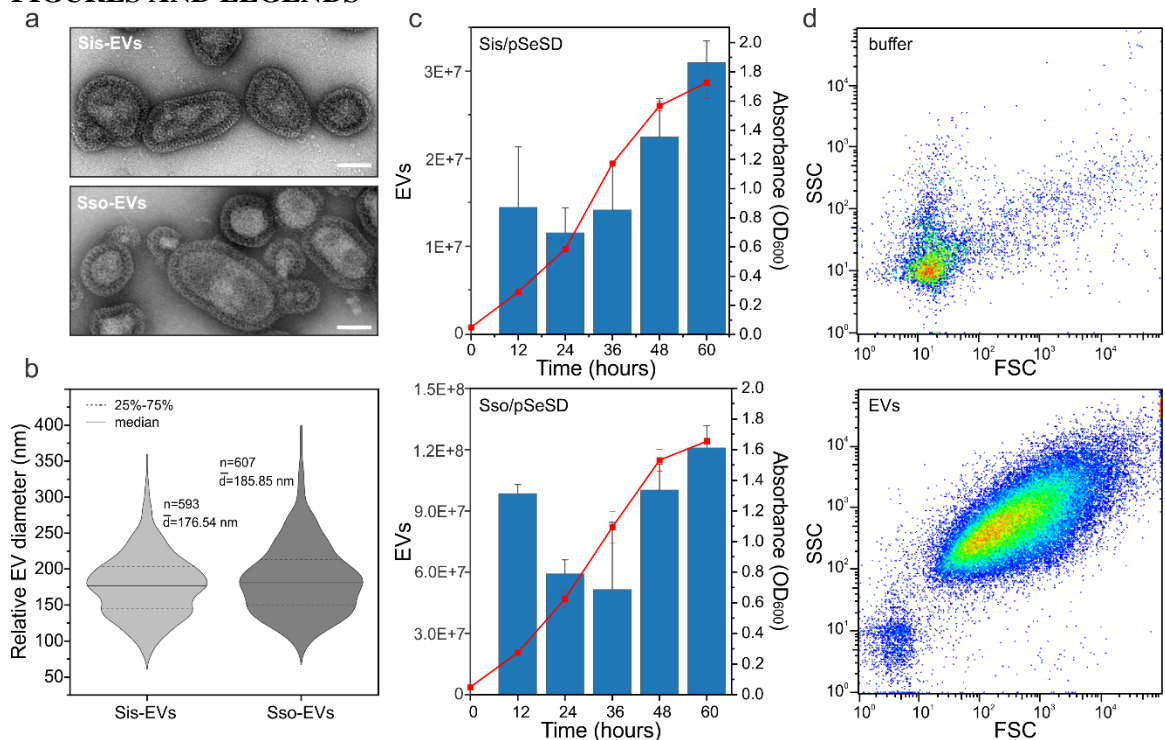
693 85. Blokesch M. Natural competence for transformation. *Curr Biol.* 2016; 26:R1126-R1130.

694 86. Hileman TH, Santangelo TJ. Genetics techniques for *Thermococcus kodakarensis*. *Front Microbiol.*
695 2012; 3:195.

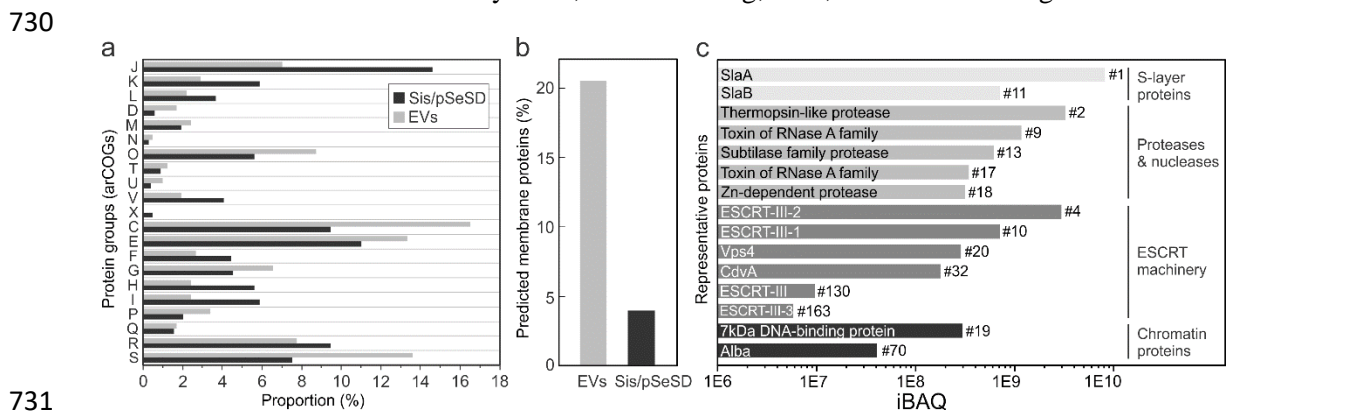
- 696 87. Stedman KM, She Q, Phan H, Holz I, Singh H, Prangishvili D *et al.* pING family of conjugative plasmids
697 from the extremely thermophilic archaeon *Sulfolobus islandicus*: insights into recombination and
698 conjugation in Crenarchaeota. *J Bacteriol.* 2000; 182:7014-20.
- 699 88. Martusewitsch E, Sensen CW, Schleper C. High spontaneous mutation rate in the hyperthermophilic
700 archaeon *Sulfolobus solfataricus* is mediated by transposable elements. *J Bacteriol.* 2000; 182:2574-
701 81.
- 702 89. Alkhatatbeh MJ, Enjeti AK, Baqar S, Ekinici EI, Liu D, Thorne RF *et al.* Strategies for enumeration of
703 circulating microvesicles on a conventional flow cytometer: Counting beads and scatter parameters. *J*
704 *Circ Biomark.* 2018; 7:1849454418766966.
- 705 90. Inglis HC, Danesh A, Shah A, Lacroix J, Spinella PC, Norris PJ. Techniques to improve detection and
706 analysis of extracellular vesicles using flow cytometry. *Cytometry A.* 2015; 87:1052-63.
- 707 91. Langmead B, Salzberg SL. Fast gapped-read alignment with Bowtie 2. *Nat Methods.* 2012; 9:357-9.
- 708 92. Desvillechabrol D, Bouchier C, Kennedy S, Cokelaer T. Sequana coverage: detection and
709 characterization of genomic variations using running median and mixture models. *Gigascience.* 2018;
710 7.
- 711 93. Tran F, Boedicker JQ. Plasmid characteristics modulate the propensity of gene exchange in bacterial
712 vesicles. *J Bacteriol.* 2019; 201:e00430-18.
- 713 94. Robertson J, McGoverin C, Vanholsbeeck F, Swift S. Optimisation of the protocol for the
714 LIVE/DEAD((R)) BacLight(TM) bacterial viability kit for rapid determination of bacterial load. *Front*
715 *Microbiol.* 2019; 10:801.
- 716 95. Leuko S, Legat A, Fendrihan S, Stan-Lotter H. Evaluation of the LIVE/DEAD BacLight kit for detection of
717 extremophilic archaea and visualization of microorganisms in environmental hypersaline samples. *Appl*
718 *Environ Microbiol.* 2004; 70:6884-6.

719

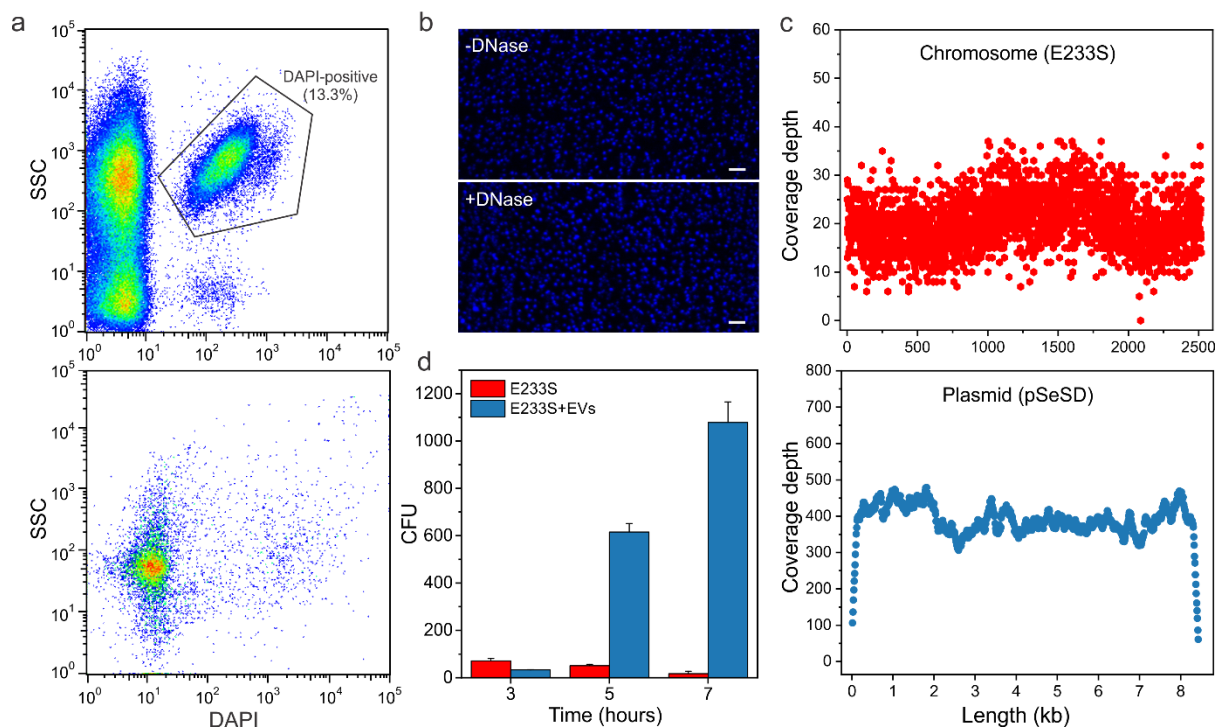
720 **FIGURES AND LEGENDS**



721
722
723 **Fig. 1.** Characterization of the *Sulfolobus islandicus* EVs. **a** Transmission electron micrographs of
724 negatively stained Sis-EVs (top) and Sso-EVs (bottom). Scale bars, 100 nm. **b** Violin plots showing the
725 size distributions of Sis-EVs (n=593) and Sso-EVs (n=607). The width of the distribution corresponds to
726 the frequency of occurrence. **c** Growth curves of *S. islandicus* E233S and *S. solfataricus* PH1-16 harboring
727 the vector pSeSD, and quantification of EVs released at indicated time points. Error bars represent standard
728 deviation from three independent experiments. **d** Quantification of Sis-EVs by flow cytometry. Top panel
729 shows the control with buffer only. SSC, side scattering; FSC, forward scattering.



731
732 **Fig. 2.** Analysis of the Sis-EV protein content. The EVs were collected during the exponential growth phase
733 (24 h) of Sis/pSeSD, purified on sucrose gradient, treated with DNase I and subjected to mass spectrometry
734 analysis. **a** Functional classification of proteins identified in highly purified Sis-EVs using archaeal clusters
735 of orthologous groups (arCOGs). arCOG categories are indicated with capital Roman letters, with the
736 annotation provided in Table S1. **b** Fraction of proteins with predicted transmembrane domains in Sis-EV
737 and cellular (Sis/pSeSD) proteomes. **c** Label-free intensity-based absolute quantification (iBAQ) of selected
738 Sis-EV proteins (the corresponding functional categories are indicated on the right). Numbers next to each
739 bar indicate the abundance rank.

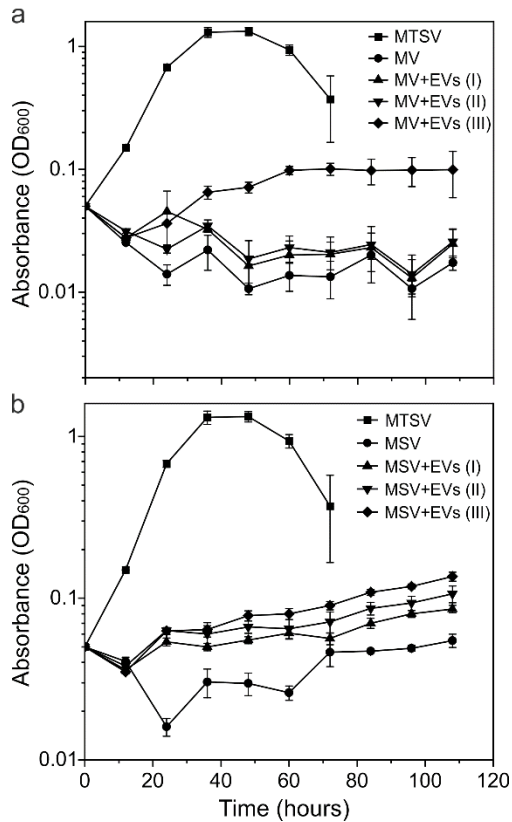


741

742

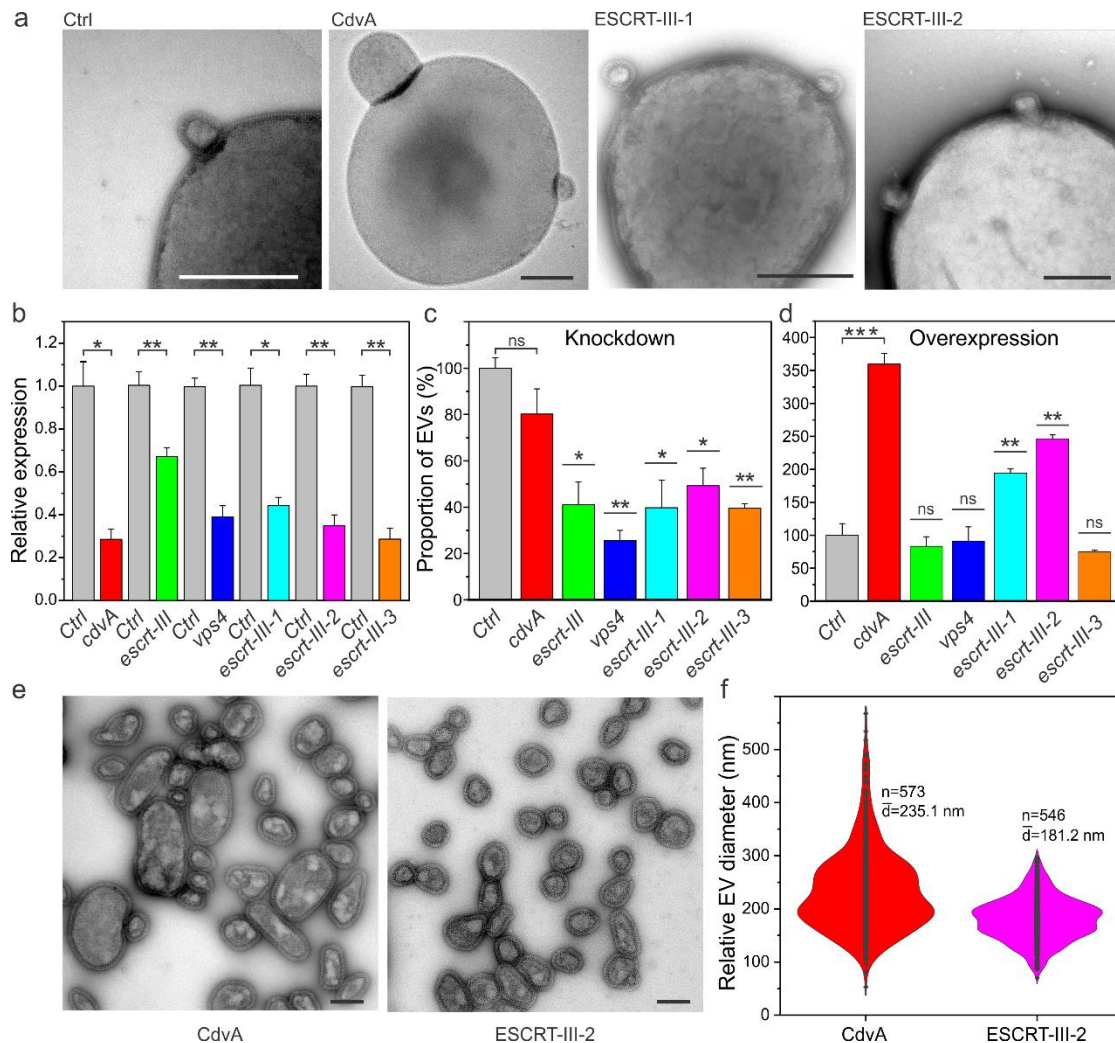
743 **Fig. 3.** Sis-EVs promote gene transfer. **a** Analysis of DAPI-stained Sis-EVs isolated from Sis/pSeSD (upper
 744 panel) by flow cytometry. All the events are shown, with the selected region indicating the DAPI-positive
 745 EVs harboring DNA. Note that most EVs are DAPI-negative. Bottom panel shows the control with the
 746 DAPI-containing buffer only. SSC, side scattering. **b** Fluorescence micrographs of DAPI-stained Sis-EVs
 747 prior (top) and after (bottom) DNase I treatment. Bar, 2 μm . **c** Sequencing depth across the chromosomal
 748 DNA (E233S) and plasmid (pSeSD). Each dot represents sequencing depth at the indicated position of the
 749 corresponding replicon. **d** Gene/plasmid transfer by Sis-EVs. Sis-EVs were treated with DNase I and then
 750 mixed with E233S cells, incubated for 3, 5 and 7 h and plated on selective plates. In the control experiment,
 751 E233S cells were mixed with the equal volume of PBS buffer. The number of obtained colony forming
 752 units (CFU) is plotted on the y-axis. Error bars represent standard deviation from three independent
 753 experiments.

754



755
756

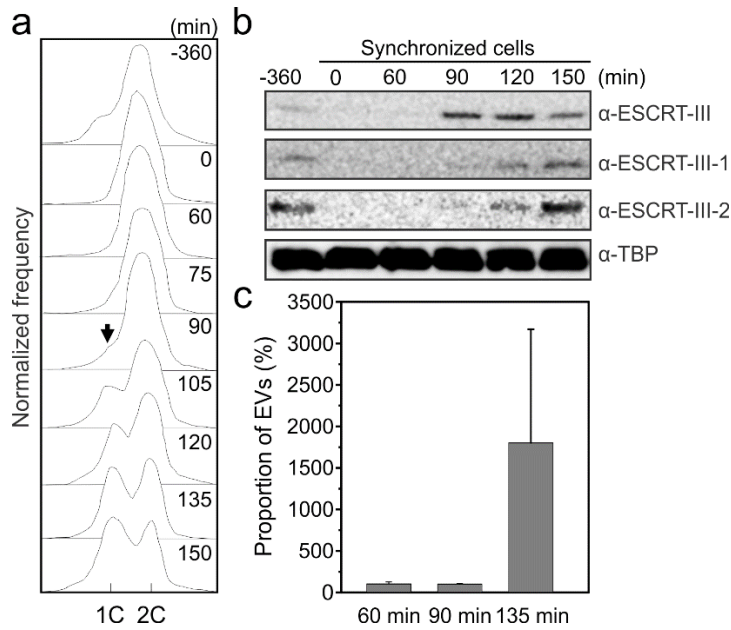
757 **Fig. 4.** Sis-EVs support heterotrophic growth of *Sulfolobus* cells. **a** Growth curves of *S. islandicus* REY15A
 758 in MV (M: mineral salts, V: vitamin mix) solution lacking organic carbon and nitrogen sources; MV
 759 solution supplemented with 1.5 ml preparations containing different amounts of EVs (MV+EVs): 24.8 μg
 760 for I, 49.6 μg for II, and 74.4 μg for III; and rich medium (MTSV), which in addition to MV solution
 761 contains 0.2% (wt/vol) sucrose (S) and 0.2% (wt/vol) tryptone (T). There was significant increase (two
 762 paired t-test, $p < 0.05$) in optical density (OD_{600}) of REY15A cells in the MV solution supplemented with
 763 EVs (III), as compared to the control culture lacking EVs. **b** Growth curves of *S. islandicus* REY15A in
 764 MSV (M: mineral salts, S: sucrose, V: vitamin mix) medium lacking organic nitrogen source; MSV medium
 765 supplemented with different concentrations of EVs (MSV+EVs), and rich MTSV medium. There was
 766 significant increase (two paired t-test, $p < 0.05$) in optical density (OD_{600}) of REY15A cells in the MSV
 767 medium supplemented with EVs, as compared to the control culture lacking EVs. Error bars represent
 768 standard deviations from three independent experiments.



769

770 **Fig. 5.** ESCRT-dependent biogenesis of Sis-EVs. **a** Representative transmission electron micrographs
 771 showing EV budding from *S. islandicus* strains overexpressing indicated proteins. Ctrl: control E233S cells
 772 carrying empty vector pSeSD. Bars, 400 nm. **b** RT-qPCR analysis of the RNA interference efficiency. Stars
 773 indicate the significance levels based on the paired two-tailed t-test. The p-values are 0.01512, 0.00514,
 774 0.00737, 0.0146, 0.00883, 0.00733, respectively. Error bars represent standard deviation from three
 775 independent experiments. **c** Quantification of Sis-EVs released from strains in which different ESCRT
 776 machinery components were depleted by CRISPR targeting. Stars indicate the significance levels based on
 777 the paired two-tailed t-test. The p-values are 0.01047, 0.00316, 0.02337, 0.01763 and 0.00177. ns, non-
 778 significant. Error bars represent standard deviation from three independent experiments. **d** Quantification
 779 of Sis-EVs released from strains overexpressing indicated ESCRT machinery components. Stars indicated
 780 the significance levels based on the paired two-tailed t-test. The p-values are 0.001, 0.0094 and 0.00435.
 781 ns, non-significant. Error bars represent standard deviation from three independent experiments. **e**
 782 Representative transmission electron micrographs of negatively stained Sis-EVs isolated from cells
 783 overexpressing CdvA and ESCRT-III-2. Bars, 200 nm. **f** Violin plots showing the size distributions of Sis-
 784 EVs isolated from cells overexpressing CdvA (n=573) and ESCRT-III-2 (n=546). The width of the
 785 distribution corresponds to the frequency of occurrence.

786



787
788

789 **Fig. 6.** EV biogenesis is linked to cell division. **a** Flow cytometry analysis of samples taken at the indicated
 790 time points during the progression of a synchronized culture of *S. islandicus*. The positions of peaks
 791 corresponding to one chromosome copy (1C) and 2C genome contents are indicated. Black arrow indicated
 792 the reappearance of the peak corresponding to the 1C genome content, signifying cell division. **b** Western
 793 blot analysis of synchronized cells. Cells ($\sim 1 \times 10^9$) were collected at indicated time points and expression
 794 of ESCRT-III, ESCRT-III-1 and ESCRT-III-2 was analyzed using the corresponding antibodies. Tata-
 795 binding protein (TBP) was used as a loading control. **c** Flow cytometry analysis of Sis-EV production by
 796 synchronized Sis/pSeSD cells at different time points after removal of acetic acid: 60 min (prior to onset of
 797 cell division), 90 min (onset of cell division) and 135 min (active cell division). Error bars represent
 798 standard deviation from three independent experiments.
 799

SUPPLEMENTARY INFORMATION

Archaeal extracellular vesicles are produced in an ESCRT-dependent manner and promote gene transfer and nutrient cycling in extreme environments

Junfeng Liu^{1,2}, Virginija Cvirkaite-Krupovic², Pierre-Henri Commere³, Yunfeng Yang¹, Fan Zhou¹, Patrick Forterre², Yulong Shen¹, Mart Krupovic^{2*}

¹ CRISPR and Archaea Biology Research Center, State Key Laboratory of Microbial Technology, Microbial Technology Institute, Shandong University, Qingdao, China

² Archaeal Virology Unit, Institut Pasteur, 75015 Paris, France

³ Institut Pasteur, Flow Cytometry Platform, 75015 Paris, France

* – Correspondence to:

Mart Krupovic
Archaeal Virology Unit,
Department of Microbiology, Institut Pasteur,
75015 Paris, France
E-mail: mart.krupovic@pasteur.fr
Tel: 33 (0)1 40 61 37 22

Running title:

Role of extracellular vesicles in extreme environments

SUPPLEMENTARY METHODS

Cell cycle synchronization

S. islandicus cells were synchronized as previously described for *S. acidocaldarius* [1, 2], with some modifications. Specifically, Sis/pSeSD cells were first grown aerobically at 75°C with shaking (145 rpm) in 30 ml of STV medium. When the OD₆₀₀ reached 0.6-0.8, the cells were transferred into 300 ml MTSV medium with an initial OD₆₀₀ of 0.05. When the OD₆₀₀ reached 0.15-0.2, acetic acid (final concentration, 6 mM) was added into the cell culture for 6 h, resulting in cell cycle arrest at the end of the DNA synthesis phase (S phase). Then, the cells were pelleted down at 5,000 rpm for 15 min at room temperature to remove the acetic acid and washed once with 0.7% (wt/vol) sucrose. Finally, the cells were resuspended into 300 ml of the pre-warmed MTSV medium.

Detection of EVs in environmental samples

Hot spring water samples collected from the solfataric field of the Campi Flegrei volcano in Pozzuoli, Italy have been described previously [3]. Twelve milliliters of the sample were concentrated by ultracentrifugation at 38,000 rpm (SW41 rotor) at 15°C for 3 h. After centrifugation, most of the supernatant was removed and the pellet was resuspended in the residual liquid (~300 µl). The concentrated sample was prepared for TEM analysis as described above.

Cell cycle and cell size analysis by flow cytometry

The cell cycle of synchronized cells and the cell sizes of knockdown and over-expression strains were analyzed by flow cytometry. Around 0.6×10^8 cells were collected for flow cytometry analysis. Briefly, cells at indicated time points were pelleted at 6,000 rpm for 5 min, resuspended in 300 µl of PBS, and then 700 µl of cool ethanol were added for at least 12 h to fix the cells. The fixed cells were then pelleted at 2,800 rpm for 20 min and washed with 1 ml of PBS. Finally, the cells were pelleted and resuspended in 80 µl of staining buffer containing 40 µg/ml propidium iodide (PI). After staining for 30 min, the DNA content or cell sizes were analyzed using the ImageStreamX MarkII Quantitative imaging analysis flow cytometry (Merck Millipore, Germany), which was calibrated with non-labeled beads with a diameter of 2 µm. The data from analysis of at least 100,000 cells was collected from each sample and analyzed with the IDEAS data analysis software.

EV-mediated gene transfer

EVs isolated and purified from 6 L of exponentially growing Sis/pSeSD culture (24 h) were used for gene transfer experiments as described previously [4], with some modification. Briefly, E233S cells were grown in 30 ml of MTSVU medium until optical density reached 0.2 and then harvested by centrifugation (7,000 rpm for 10 min at room temperature). The cell pellet was washed 6 times with 30 ml of 0.7% (wt/vol) sucrose solution to remove the uracil and then resuspended in 30 ml of MCSV. One ml of EV preparation (76 µg/ml based on the total protein amount) or PBS (control) were added to 5 ml of E233S cell culture. The cells were incubated at 75°C with shaking (145 rpm). After 3 h, 5 h and 7 h of incubation 100 µl of each sample were collected and serial dilutions were spread on the pre-warmed MCSV plates and incubated at 75°C. After 10 days of incubation, single colonies were picked, inoculated into nuclease free water and 2 µl were used as template for PCR with plasmid-specific primers pSeSD-F and pSeSD-R (Table S5) to check for the presence of pSeSD plasmid.

Determination of the relative EV diameters

Due to pleomorphicity of EVs, their relative diameters were determined by measuring the corresponding area (A) using ImageJ. First, the electron micrographs of negatively stained EVs were opened in ImageJ and the scale of each image was set according to the scale bar in the corresponding micrograph. Then the area of each EV was measured separately and the relative diameter (D) was calculated according to the area, based on the equation $A = (\pi/4) \times D^2$.

Live/Dead staining and fluorescence microscopy analysis

Live/Dead staining was carried out using the LIVE/DEAD BacLight™ Bacterial Viability Kit (Invitrogen, US) [5, 6] according to the supplier's protocols. Specifically, around 0.6×10^8 cells from the cell cultures at indicated time points were pelleted at 6,000 rpm for 5 min and resuspended in 50 µl of the M (mineral salts) solution. Then, the cells were mixed with 50 µl of the 2X stock solution of the LIVE/DEAD BacLight staining reagent mixture giving the final concentrations of SYTO 9 and propidium iodide of 6 µM and 30 µM, respectively. The samples

were incubated at room temperature in the dark for 15 min, then the excess of dyes was removed by centrifugation at 6,000 for 5 min. The cells were resuspended in 80 μ l of the M solution and 5 μ l were used for fluorescence microscopy observation under the Leica TCS SP8 confocal microscope (Leica, Germany). The data was analyzed using the Leica Application Suite X imaging and analysis software (Leica, Germany).

For DAPI staining of the cells, around 0.6×10^8 cells from the cell cultures were pelleted at 6,000 rpm for 5 min and resuspended in 80 μ l of PBS staining buffer containing 9 μ M (2.5 μ g/ml) DAPI. For DAPI staining of the EVs, 50 μ l of EV preparations were mixed with the 2 \times DAPI stock solution, giving a final concentration of DAPI of 9 μ M (2.5 μ g/ml). After staining for 30 min, 5 μ l of DAPI-stained samples were used for fluorescence microscopy observation under the Leica TCS SP8 confocal microscope (Leica, Germany).

Mass spectrometry and data analysis

The total protein content (i.e., membrane-associated and soluble proteins) of the Sis/pSeSD cells and highly purified (see above) EVs were analyzed by tandem liquid chromatography–tandem mass spectrometry (LC-MS/MS). The EVs and cells were snap-frozen in liquid nitrogen, lyophilized and re-suspended in 100 μ l of lysis buffer including 8 M Guanidine HCl (GuHCl), 5 mM Tris(2-carboxyethyl)phosphine (TCEP) and 20 mM 2-chloro-acetamide (CAA). After kept at 95°C for 5 min, 900 μ l of 50 mM Tris-HCl (pH 8.0) were added to the samples to dilute GuHCl to a concentration of under 1M. Then a mixture of 500 ng of LysC/Trypsin was added to the samples and kept at 37°C overnight for digestion of the proteins. The reaction was stopped by addition of 1% formic acid. Peptides were desalted using Sep-Pac C18 Cartridges (Waters, USA), following the manufacturer's instructions. The purified peptides were concentrated to near dryness, re-suspended in 20 μ l of 0.1% formic acid and analyzed by Nano LC-MS/MS at the Proteomics Platform of Institut Pasteur (Paris, France) using an EASY-nLC 1200 system (peptides were loaded and separated on a 30 cm long home-made C18 column; Thermo Fisher Scientific, Waltham, MA, USA) coupled to a Q Exactive Plus system (Thermo Fisher Scientific) tuned to the DDA mode. Peptide masses were searched against annotated *S. islandicus* REY15A proteins using Andromeda with the MaxQuant ver. 1.3.0.543 244 software, and additionally with the X!Tandem search engine. Identified proteins were functionally annotated against the archaeal clusters of orthologous groups (arCOG) database [7].

Heterotrophic growth assay

EVs were isolated from 20 L of Sis/pSeSD cell culture and purified by ultracentrifugation in sucrose gradient as described above and resuspended in 18 ml of the M (mineral salts) solution. The final concentration of the EV preparation was 49.6 μ g/ml, based on the total protein amount. *S. islandicus* REY15A cells were cultured in MTSV medium and collected when they reached the early logarithmic phase ($OD_{600}=0.2$). The cells were washed 6 times with the M solution by centrifugation at 7,000 rpm for 10 min to remove the traces of sucrose (S) and tryptone (T). The washed cells were inoculated into 10 ml of MV, MSV and MTSV medium as the control groups, to the initial OD_{600} of 0.05. Experimental groups were each supplemented with 1.5 ml of the EV preparations containing different concentration of EVs (24.8 μ g for group I, 49.6 μ g for group II and 74.4 μ g for group III). The experiment was repeated three times.

Construction of the CRISPR type III-B-based RNA interference plasmids and RNA interference

The CRISPR type III-B-based RNA interference plasmids were constructed according to the methods described previously [8, 9]. For RNA interference, 40-nt protospacers matching the genes of interest were selected from the anti-sense strand of the corresponding genes downstream of the GAAAG, CAGAG or AAAG (5'-3') sequences and cloned into the genome-editing plasmid pGE [8]. The spacers selected and used in this study are listed in Table S4. Spacer fragments were generated by annealing the corresponding complementary oligonucleotides and inserted into pGE at the BspMI restriction site. Plasmid pGE was introduced into E233S cells by electroporation and transformants were selected on MSCV plates without uracil. RNA interference was induced by arabinose (0.2% wt/vol final concentration). For enumeration with flow cytometry, the EVs were collected from 50 ml of cell cultures during the exponential growth phase of different knockdown strains (24 h), as described above. The flow cytometry measurements were done in triplicate (Fig. S16).

RNA preparation and quantitative reverse-transcription PCR (RT-qPCR)

Cells from RNA interference (knockdown) strains were collected for RNA extraction after 24 h post induction. Total RNAs were extracted using TRI Reagent® (SIGMA-Aldrich, USA). The concentrations of the total RNAs

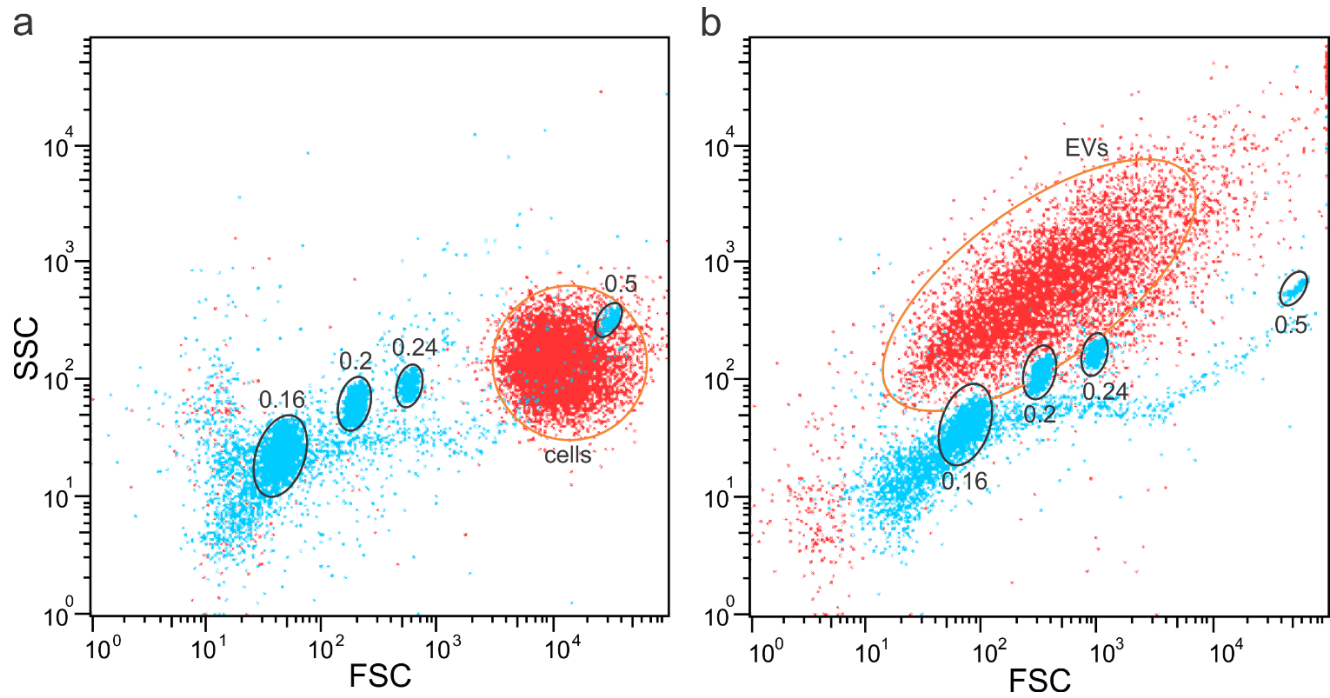
were estimated using the Eppendorf BioSpectrometer® basic (Eppendorf AG, Germany). The quality of the RNA preparations was further checked by agarose gel electrophoresis.

First-strand cDNAs were synthesized from the total RNAs according to the protocol of Maxima First Strand cDNA Synthesis Kit for RT-qPCR with dsDNase (Thermo Scientific, USA). Shortly, 2 µg of RNA were treated with the dsDNAase at 37°C and then the reverse transcription reaction was carried out by incubation for 10 min at 25°C followed by 30 min at 50°C, and finally terminated by heating at 85°C for 5 min. The resulting cDNA preparations were used to evaluate the mRNA levels of the targeted genes by qPCR (2ng of cDNA were used as the template), using Luna® Universal qPCR Master Mix (New England Biolabs, USA) and gene-specific primers (Table S5). qPCR was performed in an Eppendorf MasterCycler RealPlex⁴ (Eppendorf AG, Germany) with the following steps: denaturing at 95°C for 2 min, 40 cycles of 95°C 15 s, 55°C 15 s and 68°C 20 s. Relative amounts of mRNAs were calculated using the comparative Ct method with 16S rRNA as the reference [10]. Three independent biological experiments and three technical replicates were carried out for RT-qPCR.

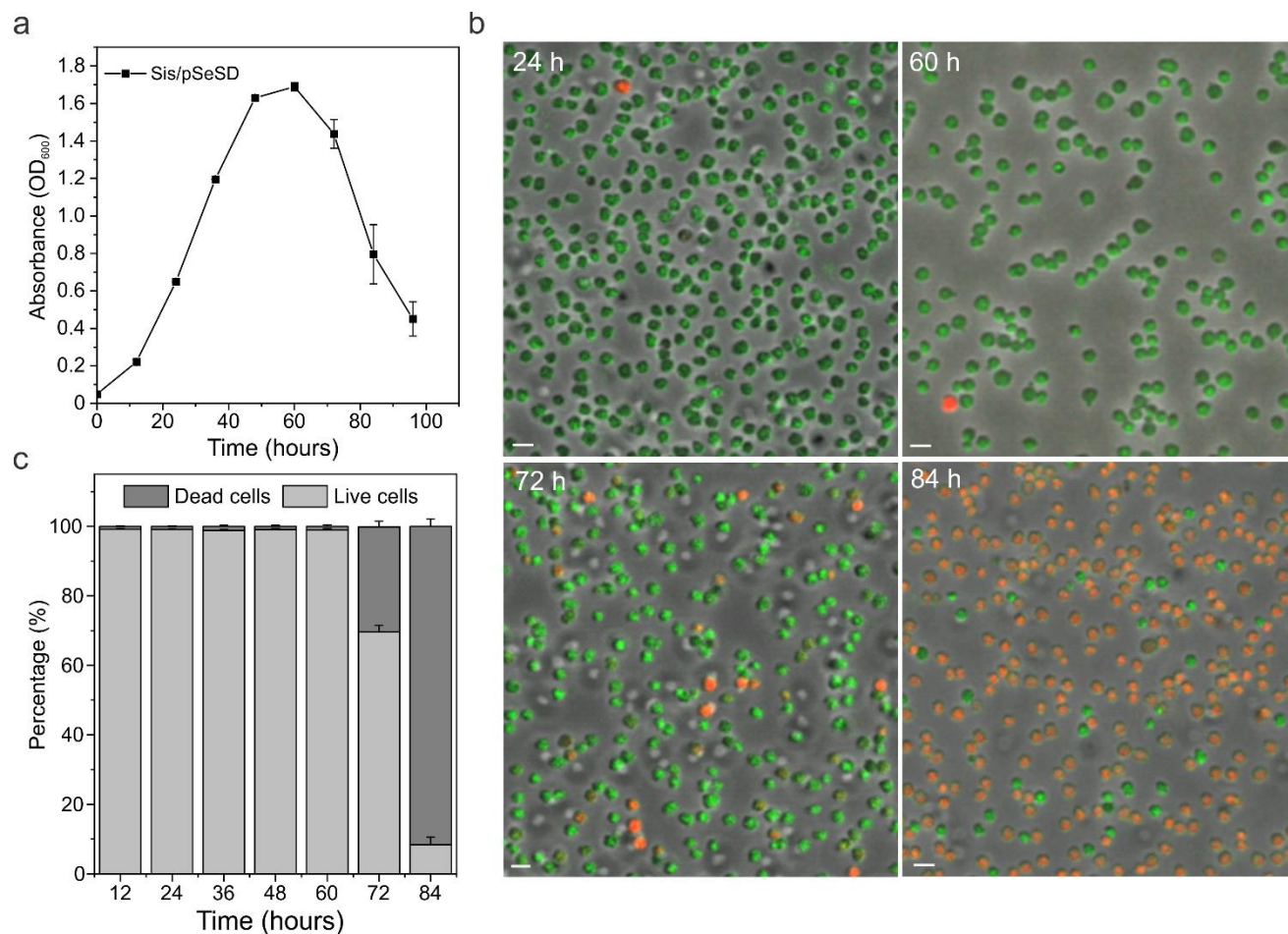
Western blot

To verify the presence of ESCRT proteins in the EVs, the sucrose-gradient purified EV samples were run in 12% polyacrylamide gel using tris-glycine running buffer, then transferred onto PVDF membrane. ESCRT proteins were detected using antibodies against ESCRT-III, ESCRT-III-1 and ESCRT-III-2 (HuaAn Biotechnology Co., Hangzhou, Zhejiang, China), as described previously [11]. The goat anti-rabbit (Thermo Fisher Scientific, USA) secondary antibodies coupled with peroxidase were used as secondary antibodies. The specific bands were detected by chemoluminescence using ECL prime western blotting detection reagents (Amersham) according to the manufacturer's instructions. Proteins purified from *E. coli* BL21-CodonPlus(DE3)-RIL (Agilent Technologies) were used as the positive controls.

SUPPLEMENTARY FIGURES

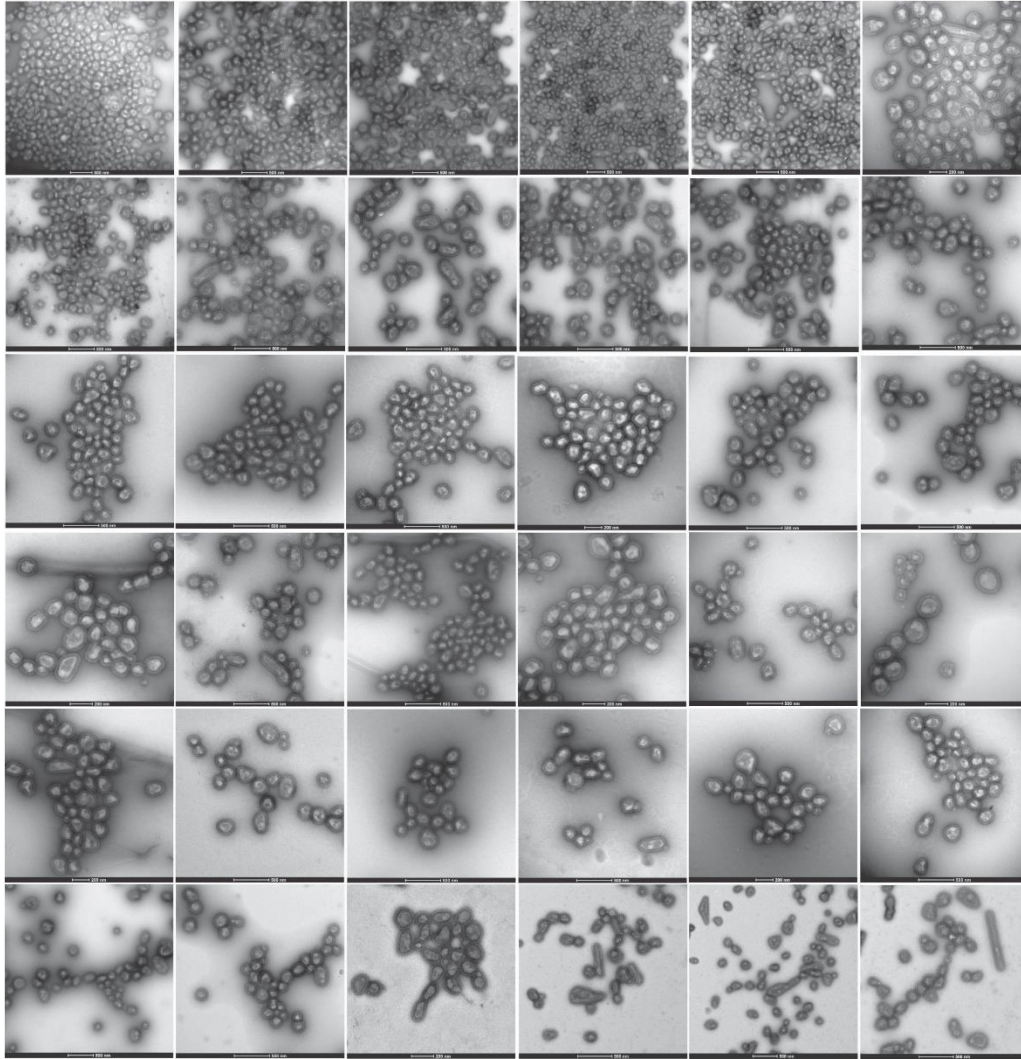


Supplementary Fig. 1. Quantification of the number of EVs by flow cytometry. **a** *S. islandicus* cells carrying pSeSD vector mixed with fluorescently-labeled beads of defined diameters (0.16-0.5 μm). **b** EV preparation mixed with beads of defined diameters (0.16-0.5 μm). Populations of cells and EVs are circled for convenience. The numbers indicate the diameter of the beads used in the flow cytometry analysis. SSC, side scattered light; FSC, forward scattered light.

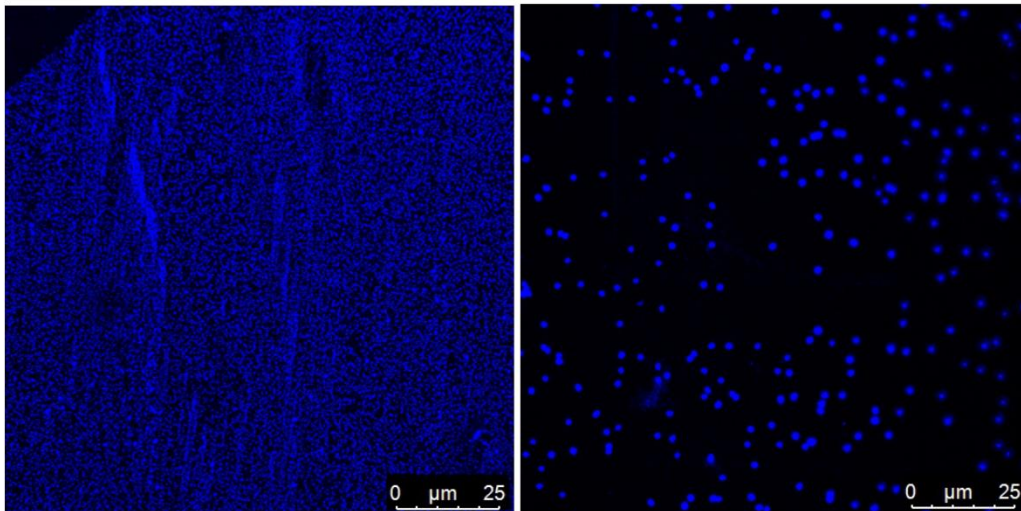


Supplementary Fig. 2. Live/dead staining of cells of Sis/pSeSD at different time points. **a** Growth curve of Sis/pSeSD. Error bars represent standard deviation from three independent experiments. **b** Ratios of live and dead cells in the population estimated using live/dead staining of Sis/pSeSD cells at different time points. Error bars represent standard deviation from three independent experiments. Around 10,000 cells were counted for each experiment at each time point to calculate the ratio between live and dead cells. **c** Representative images of the live/dead staining of Sis/pSeSD cells at indicated time points. Scale bars, 2 μ m.

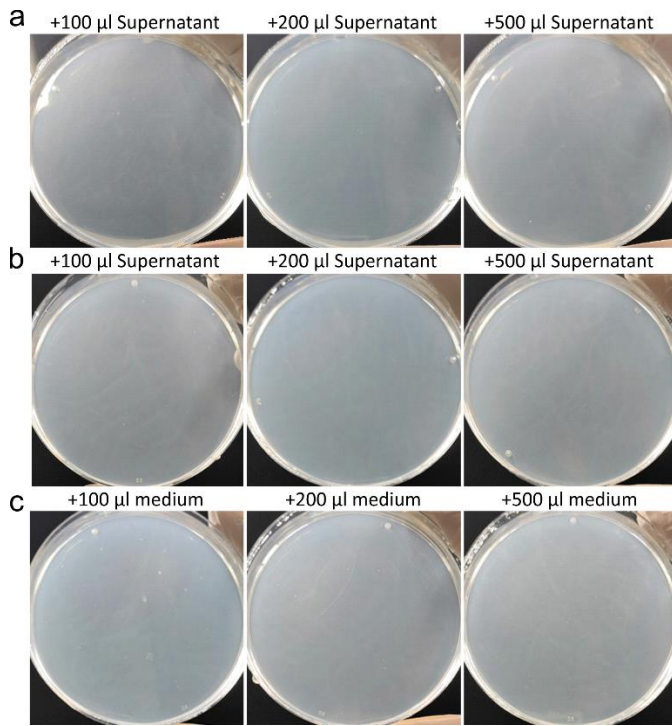
a



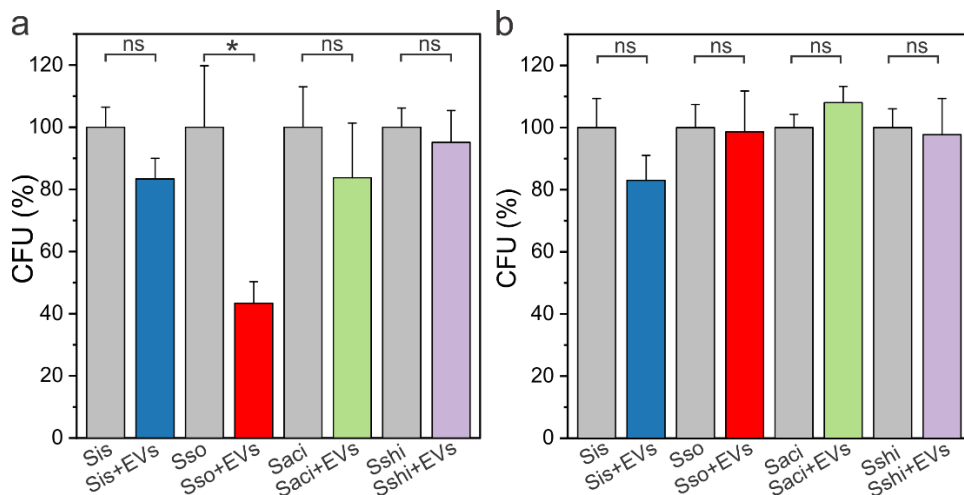
b



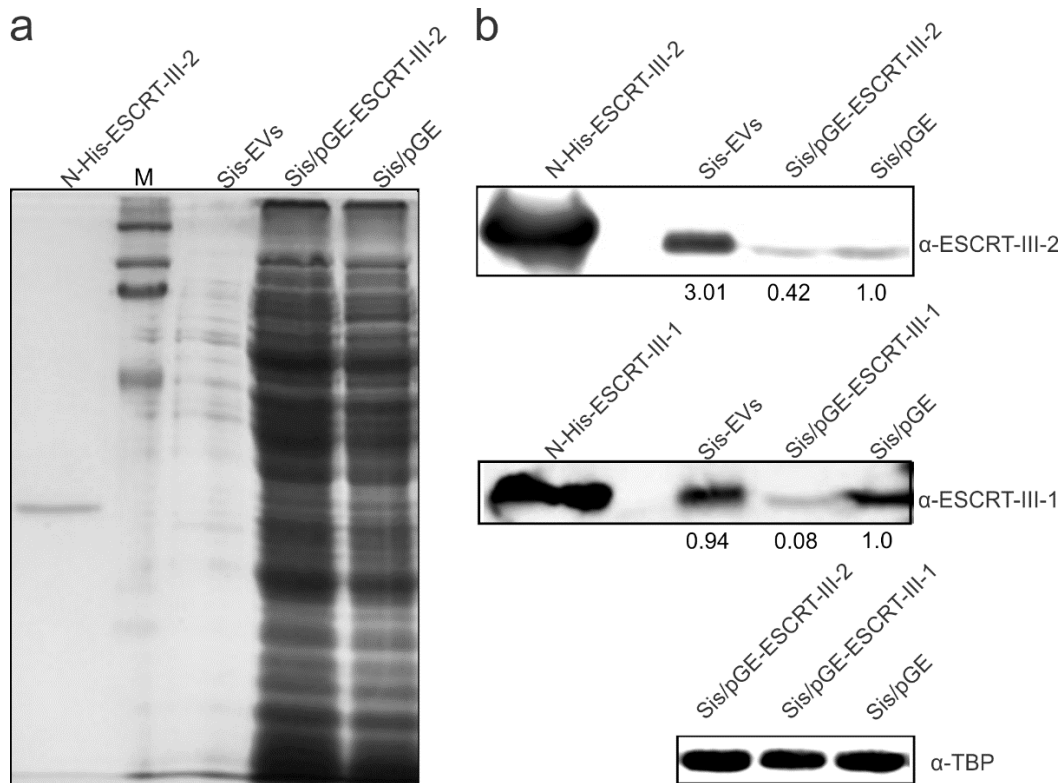
Supplementary Fig. 3. Evaluation of cellular contamination in Sis-EV preparations. **a** Thirty-six randomly acquired transmission electron micrograph of negatively stained Sis-EVs showing absence of cellular contaminants. Scale bars are shown below each micrograph. **b** Sis-EV preparation (left) and *S. islandicus* cells (right) stained with DAPI and observed under fluorescence microscope using the same magnification.



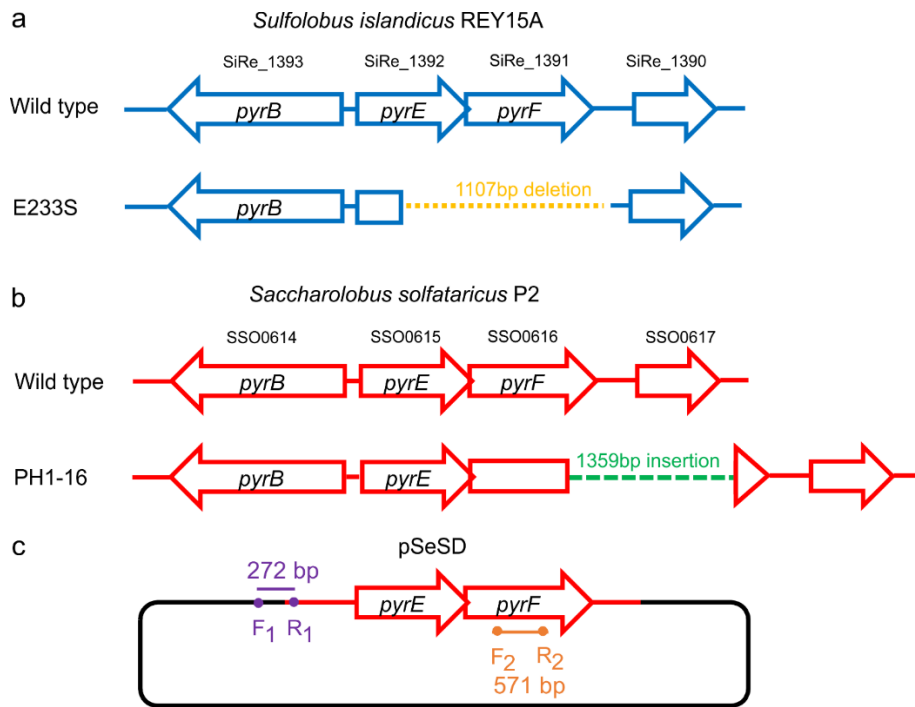
Supplementary Fig. 4. EVs do not form colonies on the plates. To evaluate the presence of cellular contaminants in the EV preparations, cell cultures of *Sulfolobus islandicus* E233S carrying pSeSD (a) or pSeSD-CdvA (b) plasmids were collected following induction with 0.2% (w/v) arabinose for 24 h, and centrifuged (7,000 rpm, 10 min, room temperature) to remove the majority of the cells. The supernatants were then filtered through 0.45 µm filter to remove the remaining cells and cell debris. Finally, 500 µl, 200 µl and 100µl of the filtered supernatants were spread on MCSV plates respectively and incubated at 75 °C. Same volumes of medium (c) were used as a control. After 10 days of incubation, no colonies formed on either of the plates, indicating that there were no cells in the filtered supernatants, whereas the large vesicles produced by the CdvA overexpression strain were not mini-cells.



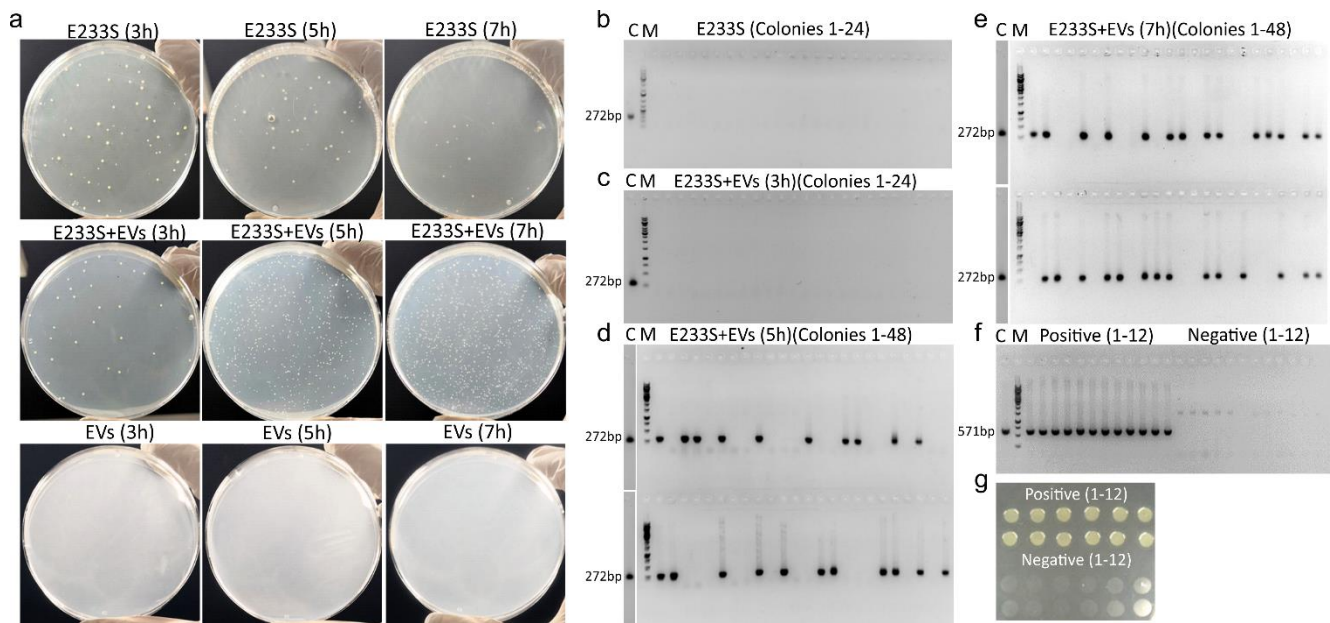
Supplementary Fig. 5. Effect of Sis-EVs on the ability of different *Sulfolobus* strains to form colonies. Sis-EVs produced by Sis/pSeSD strain were mixed with the cells, incubated for 3 (a) and 5 (b) hours and plated on rich medium. Star indicates significant difference based on the paired two-tailed t-test, $p=0.02907$. Error bars represent standard deviation from three independent experiments. Abbreviations: ns, non-significant; Sjs, *S. islandicus*; Sso, *S. solfataricus*; Saci, *S. acidocaldarius*; Sshi, *S. shibatae*.



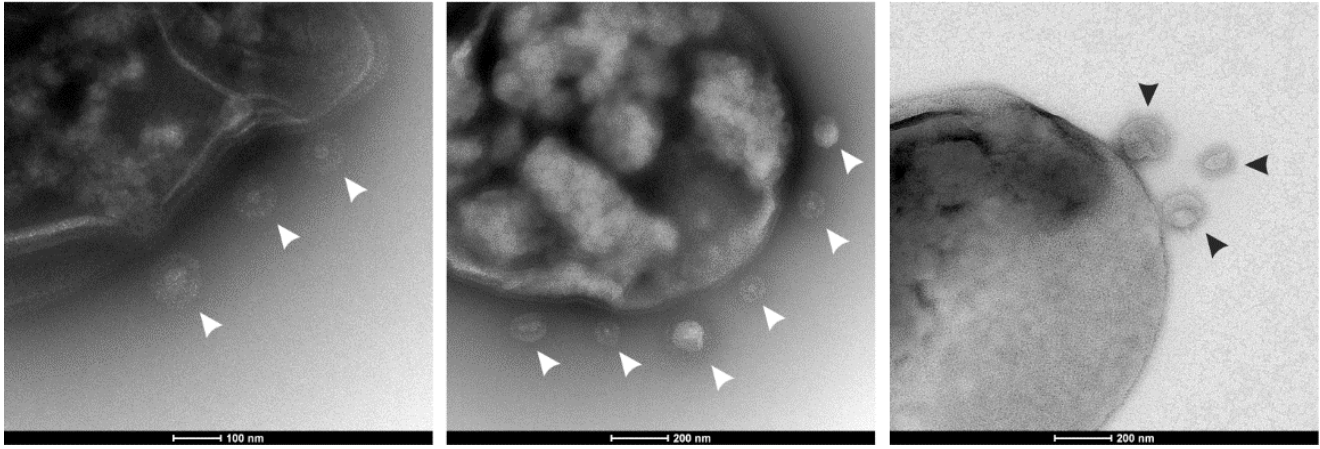
Supplementary Fig. 6. Confirmation of ESCRT-III-1 and ESCRT-III-2 presence in the Sis-EVs by western blot. ESCRT-III-2 and ESCRT-III-1 were highly enriched in Sis-EVs. **a** Coomassie blue staining of the protein gel. A total amount of 2.3 μ g of Sis-EV preparation and 0.75 mg of cells from the knockdown strain of *escrt-III-2* (Sis/pGE-ESCRT-III-2) and the cells with the empty vector (Sis/pGE) were loaded in the gel. **b** Western blot analysis of the amount of ESCRT-III-2 (top) and ESCRT-III-1 (bottom) in Sis-EVs as well as in the corresponding knockdown and control cells. N-His-ESCRT-III-2 and N-His-ESCRT-III-1 are proteins purified from the *E. coli* cells that were used as the positive controls. Anti-TBP antibodies were used as the loading control.



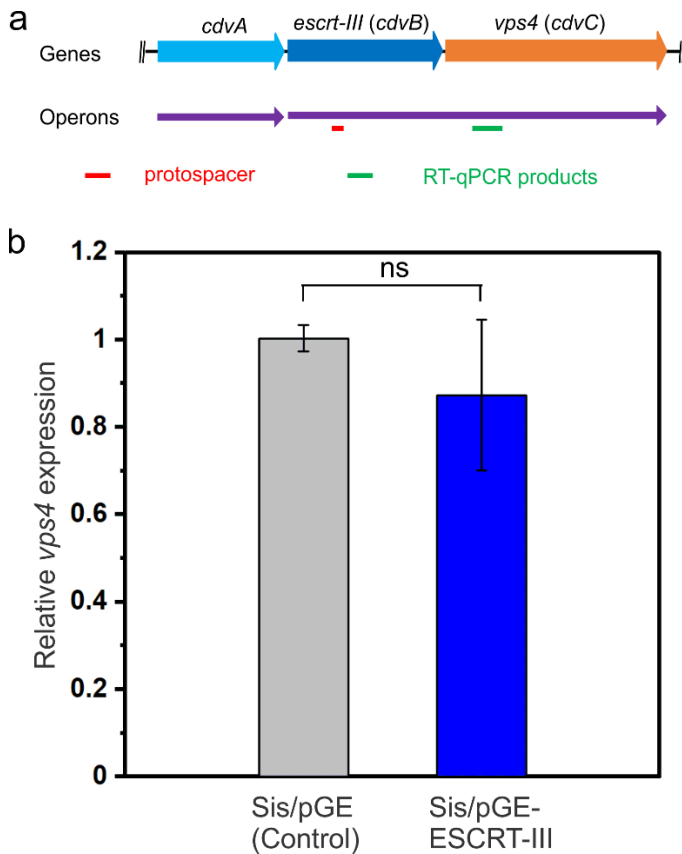
Supplementary Fig. 7. Schematic showing the genotypes of the uracil auxotroph mutants of *S. islandicus* REY15A (E233S) and *S. solfataricus* P2 (PH1-16). **a** E233S is a uracil auxotroph mutant of *S. islandicus* REY15A, carrying a 1107bp deletion including the 3'-distal 233bp of the *pyrE* gene and the entire *pyrF* gene [12]. **b** The *pyrEF* locus in the genome of *S. solfataricus* P2 and PH1-16. The latter carries a transposon insertion (1359 bp) within the *pyrF* gene[13]. **c** pSeSD is an *E. coli-Sulfolobus* shuttle vector. It contains *pyrEF* genes and their adjacent regions originating from *S. solfataricus* P2. When electroporated into E233S cells, pSeSD restores the ability of E233S cells to synthesize uracil. F1 and R1 (in purple) are the forward and reverse primers targeting the pSeSD multiple-cloning site and the adjacent region, including the arabinose-inducible promoter, start codon and terminator. F2 and R2 (in orange) are the forward and reverse primers targeting a fragment of the pSeSD *pyrF* gene. The two sets of primers were used to confirm the transfer of pSeSD plasmid into E233S cells (see Figures 3d and S8).



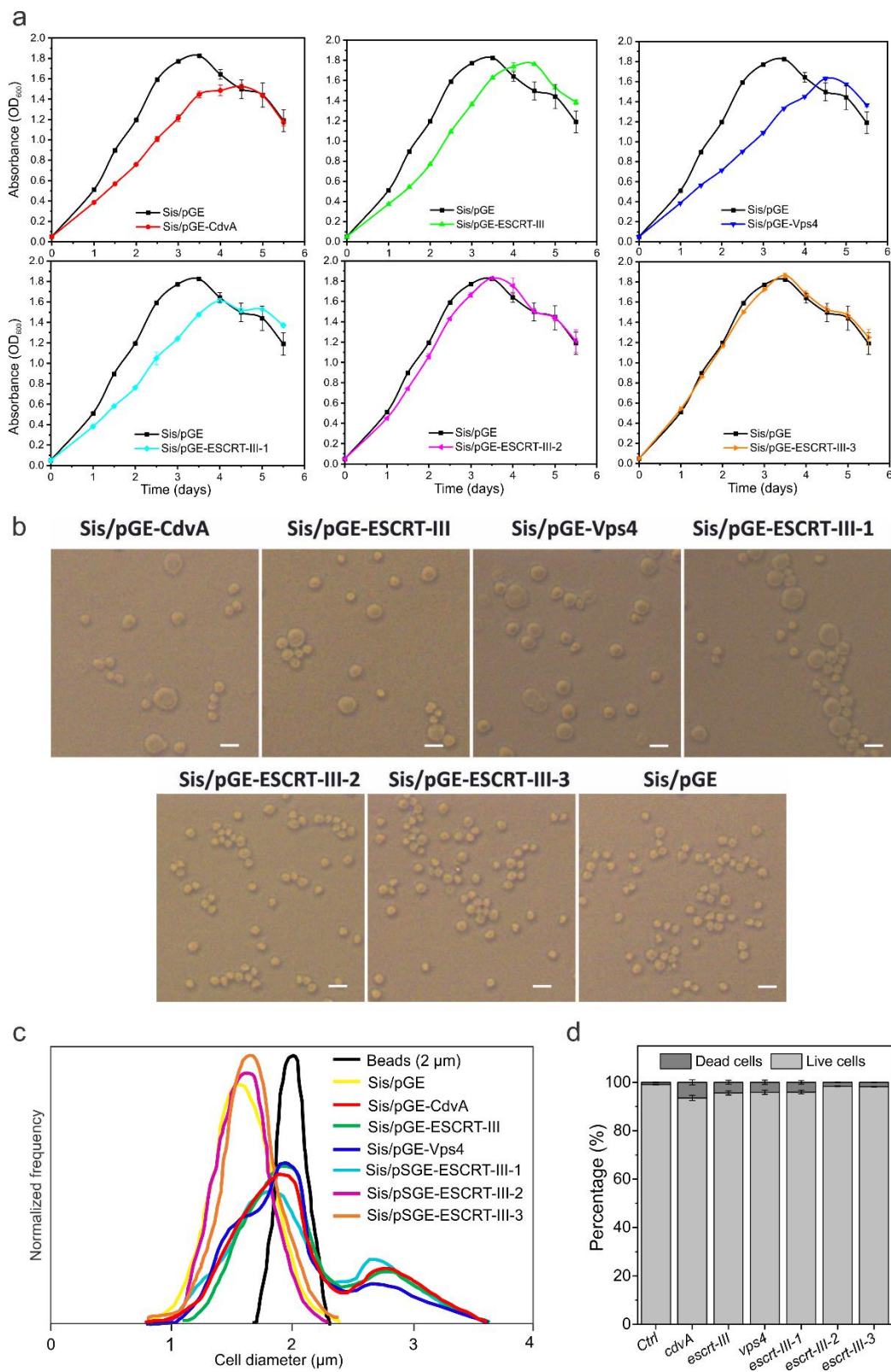
Supplementary Fig. 8. Gene transfer by Sis-EVs. **a** Representative plates showing colony formation of uracil auxotroph strain E233S without incubation with Sis-EVs (top) and after incubation with Sis-EVs for indicated time periods (middle). The bottom panel shows that no colonies were formed when purified Sis-EVs alone were plated on the uracil free plates. **b-e** PCR verification of the presence of pSeSD plasmid in the colonies described in panel **a** with the F1 and R1 primers (Fig. S6). **f** PCR verification of the *pyrF* gene presence in the isolated *S. islandicus* colonies with the F2 and R2 primers (Fig. S6). *pyrF* gene was present only in pSeSD-carrying colonies (positive 1-12); no ectopic *pyrF* integration in pSeSD-negative colonies (negative 1-12) was detected. Primer sequences used for PCR are provided in Table S5. **g** pSeSD-carrying (top 12) and pSeSD-negative (bottom 12) strains were spotted on MCSV plates without uracil; only pSeSD-carrying strains could stably grow. Abbreviations: C, positive control using pSeSD as a template (272 bp in panels b-e, primers F1-R1; 571 bp in panel f, primers R2-F2); M, size marker.



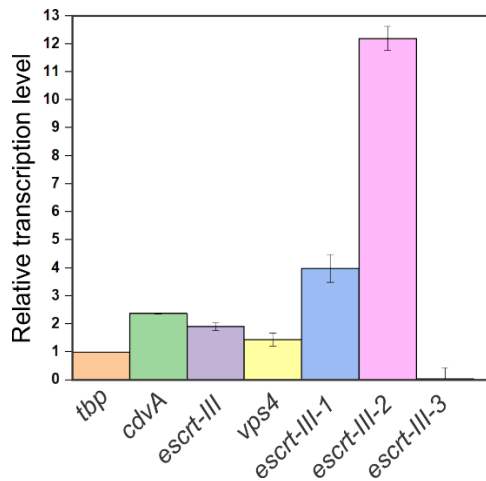
Supplementary Fig. 9. Transmission electron micrographs showing S-layer-coated EVs directly in the environmental sample. EVs are indicated with arrowheads. Scale bars are shown at the bottom of each image.



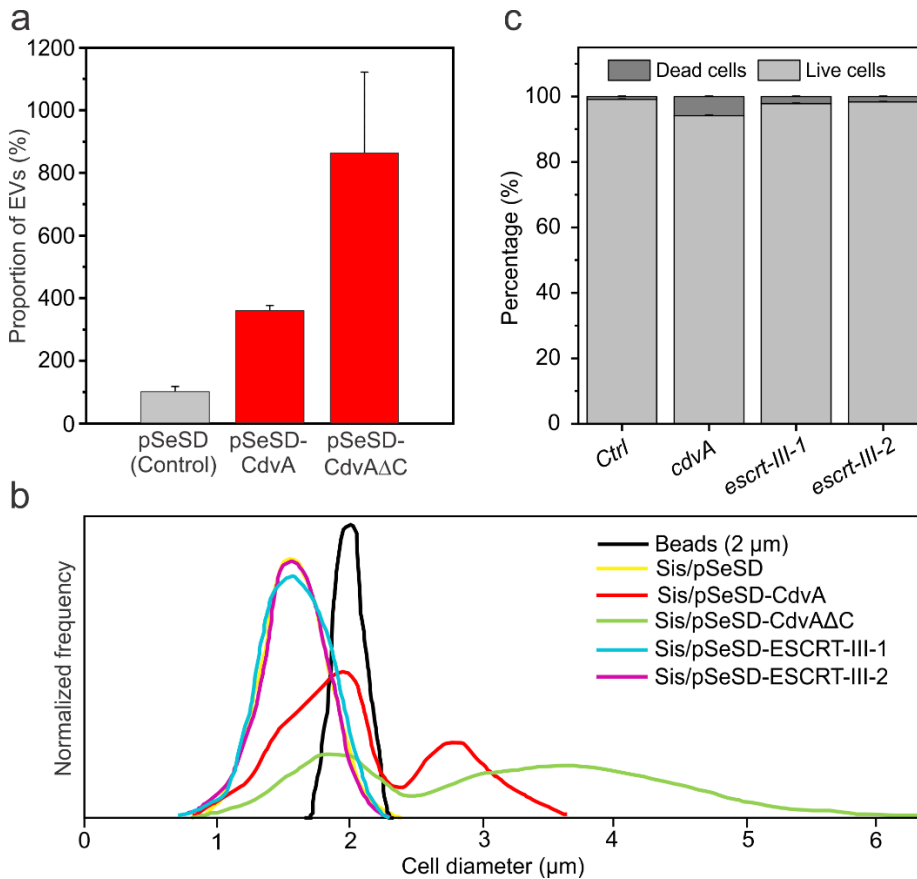
Supplementary Fig. 10. Gene silencing of *esct-III (cdvB)* does not affect the expression of the *vps4*. **a** Schematic showing the gene organization of the *Sulfolobus cdv* locus, containing *cdvA*, *esct-III (cdvB)* and *vps4 (cdvC)* genes. *esct-III* and *vps4* form a bicistronic operon [14, 15]. The location of the protospacer selected for the *esct-III* knockdown strain in this study is indicated with a red line, whereas the region amplified for the RT-qPCR analysis of the *vps4* is indicated with a green line. **b** Determination of the relative expression level of *vps4* in the control (Sis/pGE) and *esct-III* knockdown (Sis/pGE-ESCRT-III) strains by RT-qPCR. There was no significant difference of *vps4* expression in *esct-III* knockdown strain comparing with the control strain. The significance was evaluated using the paired two-tailed t-test, $p=0.2811$. ns, non-significant. Error bars represent standard deviation from three independent experiments.



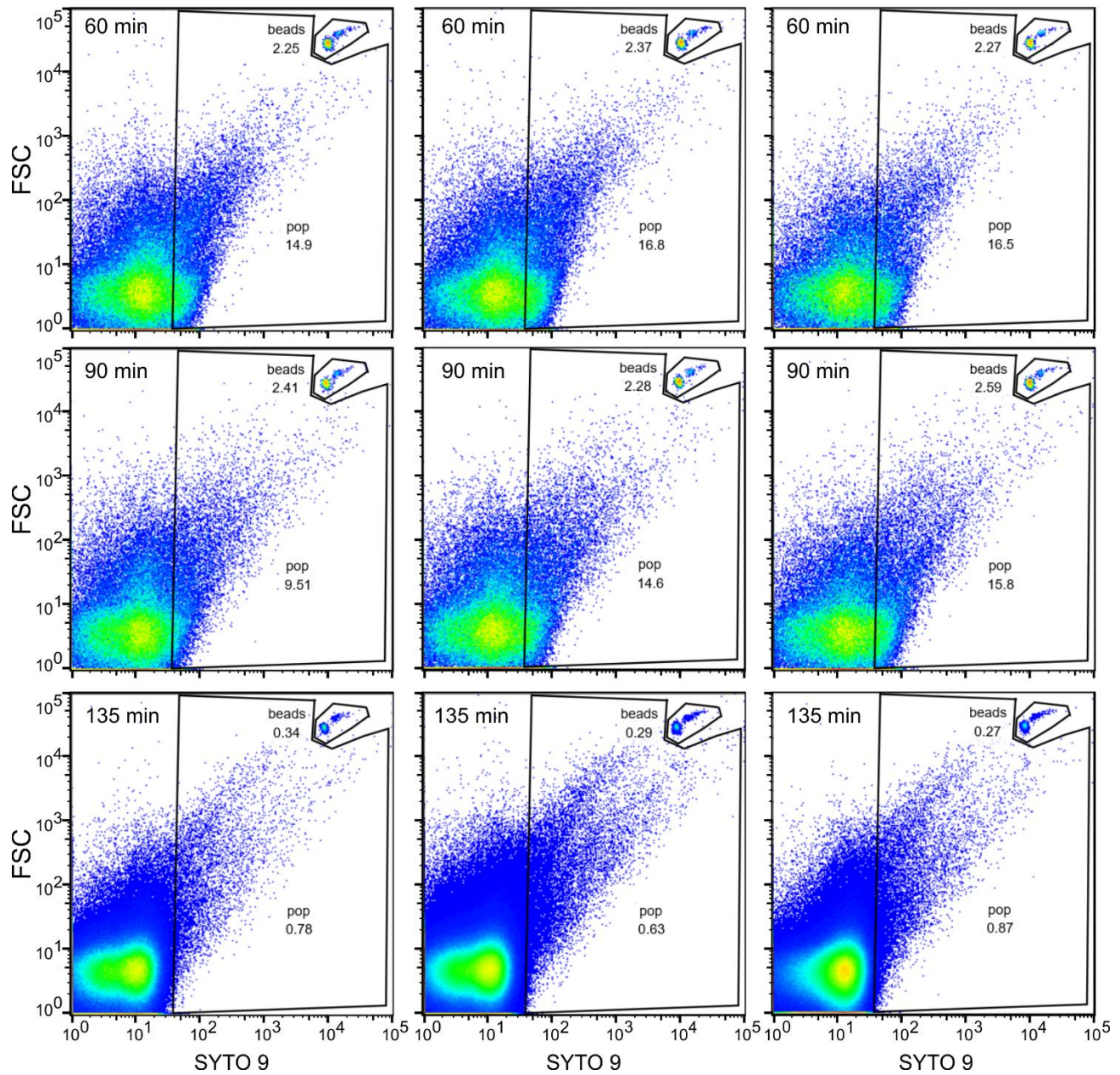
Supplementary Fig. 11. Characterization of the knockdown strains. **a** Growth curves of the knockdown strains. **b** Phase contrast micrographs of ESCRT knockdown strains. Bars, 2 μm . Strains containing an empty vector pGE were used as a negative control. **c** Cell size distribution in the knockdown cultures. Cell sizes were determined using flow cytometry as described in Materials and Methods. **d** Ratio of live and dead cells in the knockdown cultures.



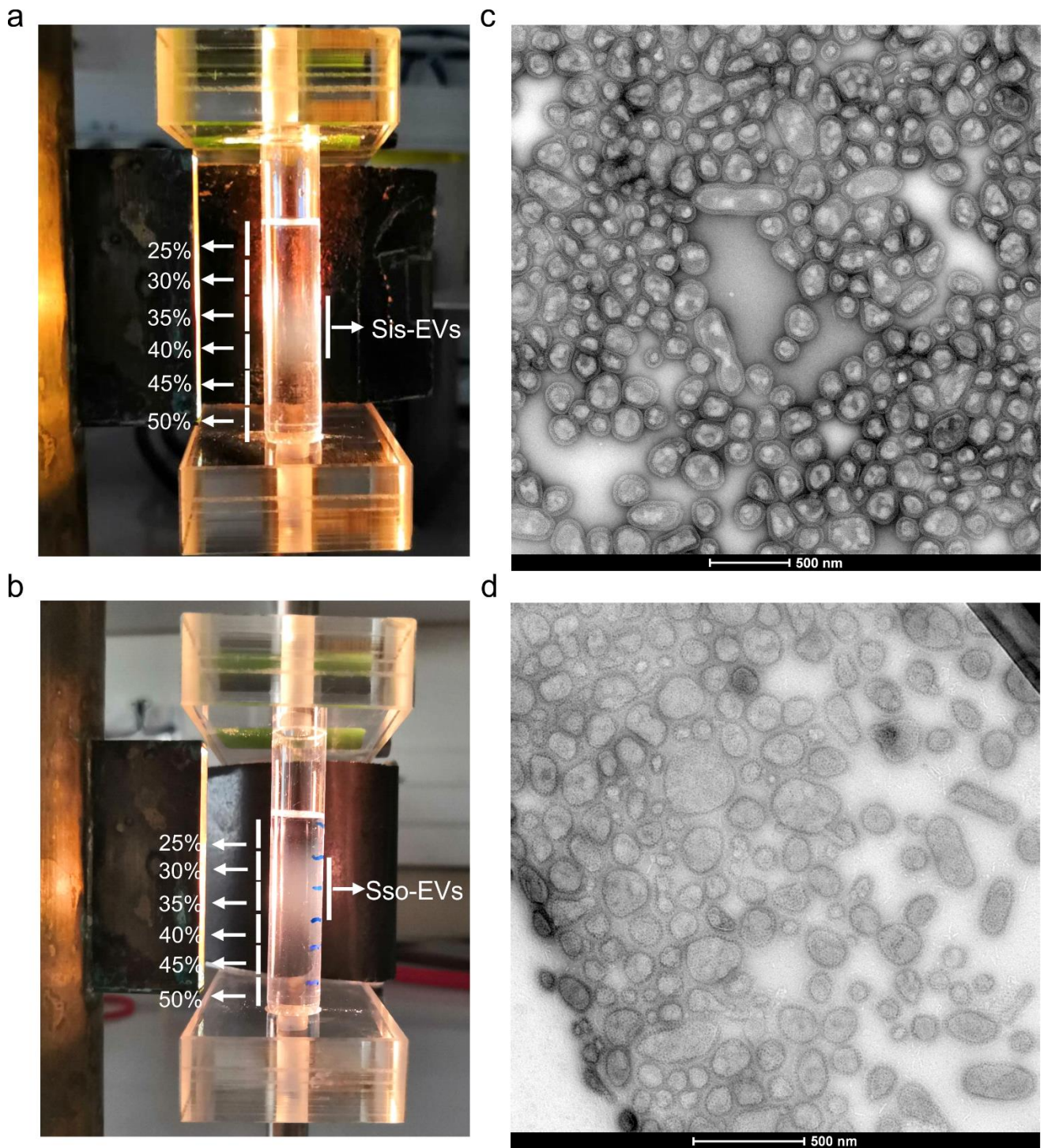
Supplementary Fig. 12. The relative expression of *escrt-III-2* is several times higher compared to other cell division genes in *S. islandicus* REY15A. For visualization purposes, the expression level of the housekeeping gene encoding TATA-binding proteins (TBP) is considered as unity, with the expression levels of all other genes calculated relative to TBP. Error bars represent standard deviation from three independent experiments.



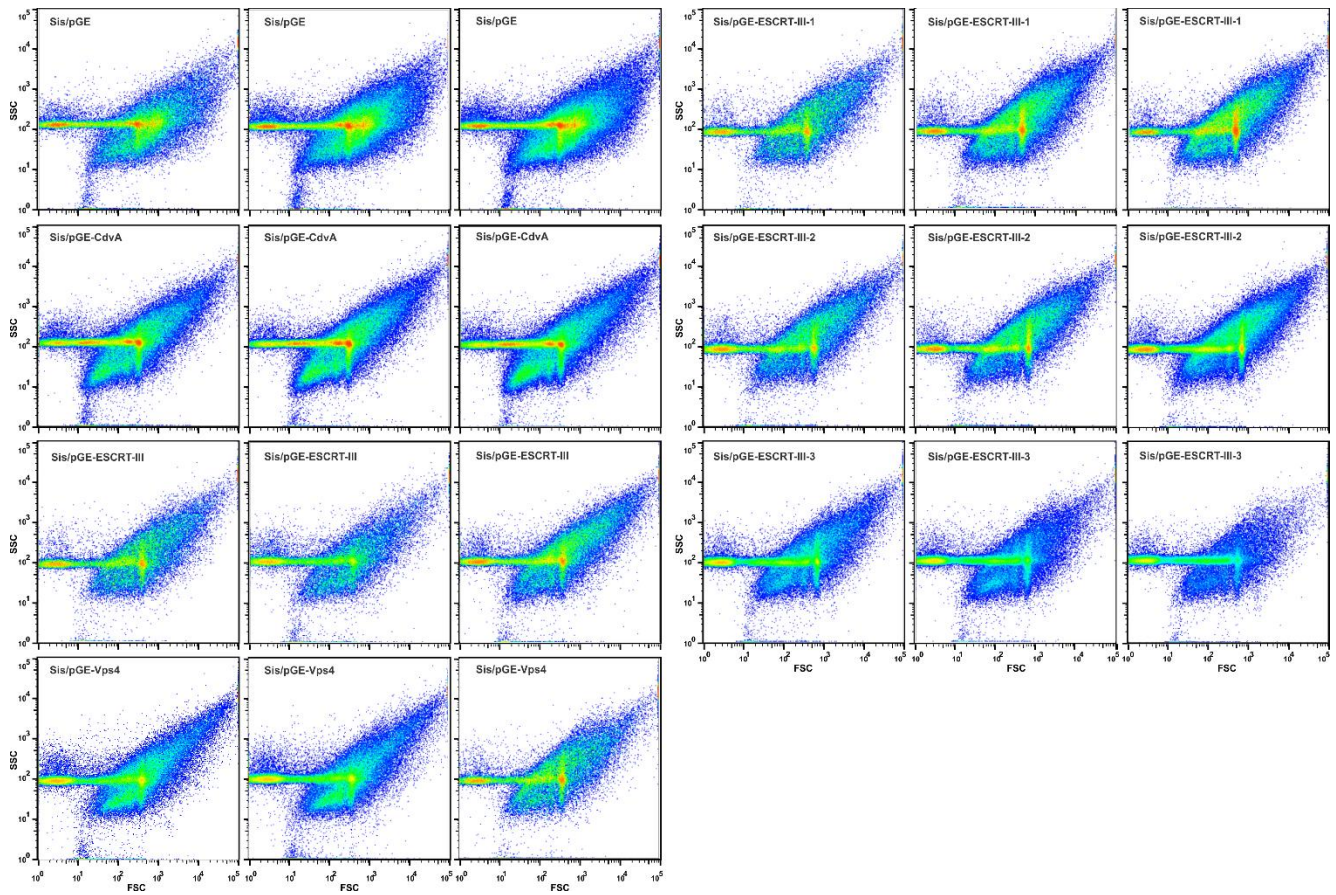
Supplementary Fig. 13. Characterization of EVs and *S. islandicus* cells overexpressing different ESCRT machinery components. **a** Quantification of the Sis-EVs released from the cells overexpressing CdvA and its C-terminally truncated mutant CdvA Δ C. Error bars represent standard deviation from three independent experiments. **b** Cell size distribution in *S. islandicus* cultures overexpressing different cell division proteins. Cell sizes were determined using flow cytometry as described in Materials and Methods. **c** Ratio of live and dead cells in the overexpression cultures.



Supplementary Fig. 14. Flow cytometry profiles of EV enumeration for synchronized Sis/pSeSD culture at different time points after removal of acetic acid. Three replicates are shown for each time point. The signal coming from the DNA-containing (SYTO9-positive) EVs is outlined. FSC, forward scattering.



Supplementary Fig. 15. EV purification by ultracentrifugation in sucrose gradient. EVs from *S. islandicus* (a) and *S. solfataricus* (b) formed opalescent bands in the 25-50% sucrose gradients in the region corresponding to 30%-40% sucrose. Transmission electron micrograph of negatively stained Sis-EVs (c) and Sso-EVs (d) collected from the corresponding opalescent bands. Scale bars, 500 nm.



Supplementary Fig. 16. Flow cytometry profiles of EV enumeration for different knockdown strains. Three replicates are shown for each strain. FSC, forward scattering; SSC, side scattering.

SUPPLEMENTARY TABLES

Table S1 Functional annotation of arCOG categories

arCOG category	Annotation
1. Information storage and processing	
J	Translation, ribosomal structure and biogenesis
A	RNA processing and modification
K	Transcription
L	Replication, recombination and repair
B	Chromatin structure and dynamics
2. Cellular processes and signaling	
D	Cell cycle control, cell division, chromosome partitioning
Y	Nuclear structure
V	Defense mechanisms
T	Signal transduction mechanisms
M	Cell wall/membrane/envelope biogenesis
N	Cell motility
Z	Cytoskeleton
W	Extracellular structures
U	Intracellular trafficking, secretion, and vesicular transport
O	Posttranslational modification, protein turnover, chaperones
X	Mobilome: prophages, transposons
3. Metabolism	
C	Energy production and conversion
G	Carbohydrate transport and metabolism
E	Amino acid transport and metabolism
F	Nucleotide transport and metabolism
H	Coenzyme transport and metabolism
I	Lipid transport and metabolism
P	Inorganic ion transport and metabolism
Q	Secondary metabolites biosynthesis, transport and catabolism
4. Poorly characterized	
R	General function prediction only
S	Function unknown

Table S2 Plasmids used in this study

Plasmid	Description	Reference
pSeSD	Empty vector for overexpression	[16]
pSeSD-CdvA	CdvA overexpression	[11]
pSeSD-CdvA Δ C	CdvA Δ C overexpression	[11]
pSeSD-ESCRT-III	ESCRT-III overexpression	[11]
pSeSD-ESCRT-III-1	ESCRT-III-1 overexpression	[11]
pSeSD-ESCRT-III-2	ESCRT-III-2 overexpression	[11]
pSeSD-ESCRT-III-3	ESCRT-III-3 overexpression	[11]
pGE	Empty vector for knockdown	[8]
pSeSD-Vps4	Vps4 overexpression	This study
pGE-CdvA	<i>cdvA</i> knockdown	This study
pGE-ESCRT-III	<i>escrt-III</i> knockdown	This study
pGE-Vps4	<i>Vps4</i> knockdown	This study

pGE-ESCRT-III-1	<i>escrt-III-1</i> knockdown	This study
pGE-ESCRT-III-2	<i>escrt-III-2</i> knockdown	This study
pGE-ESCRT-III-3	<i>escrt-III-3</i> knockdown	This study

Table S3 *Sulfolobus* strains used in this study

Strain	Phenotype	Reference
<i>S. solfataricus</i> PH1	<i>lacS:ISC1217</i>	[13]
<i>S. solfataricus</i> PH1-16	<i>pyrF:ISC1359, lacS:ISC1217</i>	[13]
<i>S. acidocaldarius</i> DSM 639	Wild type	[17]
<i>S. shibatae</i>	Wild type	[18]
<i>S. islandicus</i> REY15A	Wide type	[19]
Sis E233S	REY15A Δ <i>pyrEFAlacS</i>	[12]
Sis/pSeSD	Control for overexpression	[11]
Sis/pSeSD-CdvA	CdvA overexpression	[11]
Sis/pSeSD-CdvA Δ C	CdvA Δ C overexpression	[11]
Sis/pSeSD-ESCRT-III	ESCRT-III overexpression	[11]
Sis/pSeSD-ESCRT-III-1	ESCRT-III-1 overexpression	[11]
Sis/pSeSD-ESCRT-III-2	ESCRT-III-2 overexpression	[11]
Sis/pSeSD-ESCRT-III-3	ESCRT-III-3 overexpression	[11]
Sis/pSeSD-Vps4	Vps4 overexpression	This study

Table S4 Oligonucleotides used to construct knockdown plasmids

Name	Sequence (5'-3')	Source
CdvA-S-F	<u>AAGGCTTAAGTTCTATAGATTCTTTATCCAACGAGTCTAATCT</u>	This study
CdvA-S-R	<u>AGCAGATTAGACTCGTTGGATAAAGAATCTATAGAACTTAAGC</u>	This study
ESCRT-III-S-F	<u>AAGAAACGCCTTGCAGTTCTTGTACGGTATCTAGTTTTAGTCT</u>	This study
ESCRT-III-S-R	<u>AGCAGACTAAAAGTACGATACCGTACAAGAAGTCAAGGCGTTT</u>	This study
Vps4-S-F	<u>AAGTCCTGGAGTGTAATTGTTCTTGGTTACCTAAATTATTCT</u>	This study
Vps4-S-R	<u>AGCAGAATAATTTAGGTGAACCAAGAACAATTACACTCCAGGA</u>	This study
ESCRT-III-1-S-F	<u>AAGGCTCCTTAGAACCCTTTATTTTAAATCTCTCCTGCTCATA</u>	This study
ESCRT-III-1-S-R	<u>AGCTATGAGCAGGAGAGATTTAAAATAAAGGGTTCTAAGGAGC</u>	This study
ESCRT-III-2-S-F	<u>AAGTCCCCTGCTTCTATTACTACCTCTTGTAATCCCTCCTCTA</u>	This study
ESCRT-III-2-S-R	<u>AGCTAGAGGAGGGATTACAAGAGGTAGTAATAGAAGCAGGGGA</u>	This study
ESCRT-III-3-S-F	<u>AAGACATAATTATAAGTGCCTAACTTATTCTGCATTCTATTAA</u>	This study
ESCRT-III-3-S-R	<u>AGCTTAATAGAATGCAGAATAAGTTAGGCACTTATAATTATGT</u>	This study

Sequences added to the spacers for insertion into the BspMI restriction site of the genome editing plasmid pGE are underlined.

Table S5 Oligonucleotides used in this study

Name	Sequence (5'-3')	Source
16S-F	GAATGGGGGTGATACTGTCG	[20]
16S-R	TTTACAGCCGGGACTACAGG	[20]
ESCRT-III-F	CAGCATTCTTAGCTATTGAGAAAG	This study
ESCRT-III-R	GATAGAGTCTAAGGCTATTGC	This study
Vps4-F	GGATATAGTTCAAGCTGCACA	This study
Vps4-R	GATTAACACTTGGCATTCTGAC	This study
ESCRT-III-1-F	CGGAAAAGATTTCCAAAAGATTTG	This study
ESCRT-III-1-R	CAAGCCTACTAATCATGGAGC	This study
ESCRT-III-2-F	CGATGAAAGGAGTTATGCCAG	This study
ESCRT-III-2-R	CTTCTAATATCTTCCTTGCCTC	This study
ESCRT-III-3-F	GCTGAGCTGCTAATAGACG	This study
ESCRT-III-3-R	CTCAGACTCTCTAGCAACC	This study
Vps4-F-Nde I	GCGG <u>CATATG</u> AGTGCTCAAGTAATGCTAG	This study
Vps4-R-Sal I	TCACG <u>TCGACT</u> AATGCCTTAAACTTCTCT	This study
pSeSD-F	GCAATGTTAAACAAGTTAGGTATAC	This study
pSeSD-R	ACCTTATGTTAAACTACGCCAGT	This study
F1	CTGAGGCAGTCGAAGGATAG	This study
R1	TCGCTCTTTGCCTCACCTTG	This study
F2 (<i>pyrF</i> -F)	GCAATGGATAAACCTCTCTC	This study
R2 (<i>pyrF</i> -R)	CTGTTAATGGATTCCCTGCA	This study

SUPPLEMENTARY REFERENCES

1. Tarrason Risa G, Hurtig F, Bray S, Hafner AE, Harker-Kirschneck L, Faull P *et al.* The proteasome controls ESCRT-III-mediated cell division in an archaeon. *Science*. 2020; 369.
2. Lundgren M, Andersson A, Chen L, Nilsson P, Bernander R. Three replication origins in *Sulfolobus* species: synchronous initiation of chromosome replication and asynchronous termination. *Proc Natl Acad Sci U S A*. 2004; 101:7046-51.
3. Baquero DP, Contursi P, Piochi M, Bartolucci S, Liu Y, Cvirkaite-Krupovic V *et al.* New virus isolates from Italian hydrothermal environments underscore the biogeographic pattern in archaeal virus communities. *ISME J*. 2020; 14:1821-1833.
4. Tran F, Boedicker JQ. Plasmid characteristics modulate the propensity of gene exchange in bacterial vesicles. *J Bacteriol*. 2019; 201:e00430-18.
5. Robertson J, McGoverin C, Vanholsbeeck F, Swift S. Optimisation of the protocol for the LIVE/DEAD((R)) BacLight(TM) bacterial viability kit for rapid determination of bacterial load. *Front Microbiol*. 2019; 10:801.
6. Leuko S, Legat A, Fendrihan S, Stan-Lotter H. Evaluation of the LIVE/DEAD BacLight kit for detection of extremophilic archaea and visualization of microorganisms in environmental hypersaline samples. *Appl Environ Microbiol*. 2004; 70:6884-6.
7. Makarova KS, Wolf YI, Koonin EV. Archaeal Clusters of Orthologous Genes (arCOGs): An update and application for analysis of shared features between Thermococcales, Methanococcales, and Methanobacteriales. *Life (Basel)*. 2015; 5:818-40.
8. Li Y, Pan S, Zhang Y, Ren M, Feng M, Peng N *et al.* Harnessing Type I and Type III CRISPR-Cas systems for genome editing. *Nucleic Acids Res*. 2016; 44:e34.
9. Peng W, Feng M, Feng X, Liang YX, She Q. An archaeal CRISPR type III-B system exhibiting distinctive RNA targeting features and mediating dual RNA and DNA interference. *Nucleic Acids Res*. 2015; 43:406-17.
10. Schmittgen TD, Livak KJ. Analyzing real-time PCR data by the comparative C(T) method. *Nat Protoc*. 2008; 3:1101-8.
11. Liu J, Gao R, Li C, Ni J, Yang Z, Zhang Q *et al.* Functional assignment of multiple ESCRT-III homologs in cell division and budding in *Sulfolobus islandicus*. *Mol Microbiol*. 2017; 105:540-553.
12. Deng L, Zhu H, Chen Z, Liang YX, She Q. Unmarked gene deletion and host-vector system for the hyperthermophilic crenarchaeon *Sulfolobus islandicus*. *Extremophiles*. 2009; 13:735-46.
13. Martusewitsch E, Sensen CW, Schleper C. High spontaneous mutation rate in the hyperthermophilic archaeon *Sulfolobus solfataricus* is mediated by transposable elements. *J Bacteriol*. 2000; 182:2574-81.
14. Samson RY, Obita T, Hodgson B, Shaw MK, Chong PL, Williams RL *et al.* Molecular and structural basis of ESCRT-III recruitment to membranes during archaeal cell division. *Mol Cell*. 2011; 41:186-96.
15. Wurtzel O, Sapra R, Chen F, Zhu Y, Simmons BA, Sorek R. A single-base resolution map of an archaeal transcriptome. *Genome Res*. 2010; 20:133-41.
16. Peng N, Deng L, Mei Y, Jiang D, Hu Y, Awayez M *et al.* A synthetic arabinose-inducible promoter confers high levels of recombinant protein expression in hyperthermophilic archaeon *Sulfolobus islandicus*. *Appl Environ Microbiol*. 2012; 78:5630-7.
17. Chen L, Brugger K, Skovgaard M, Redder P, She Q, Torarinsson E *et al.* The genome of *Sulfolobus acidocaldarius*, a model organism of the Crenarchaeota. *J Bacteriol*. 2005; 187:4992-9.
18. Liu Y, Osinski T, Wang F, Krupovic M, Schouten S, Kasson P *et al.* Structural conservation in a membrane-enveloped filamentous virus infecting a hyperthermophilic acidophile. *Nat Commun*. 2018; 9:3360.
19. Guo L, Brugger K, Liu C, Shah SA, Zheng H, Zhu Y *et al.* Genome analyses of Icelandic strains of *Sulfolobus islandicus*, model organisms for genetic and virus-host interaction studies. *J Bacteriol*. 2011; 193:1672-80.
20. Sun M, Feng X, Liu Z, Han W, Liang YX, She Q. An Orc1/Cdc6 ortholog functions as a key regulator in the DNA damage response in Archaea. *Nucleic Acids Res*. 2018; 46:6697-6711.